

Economic Geology

BULLETIN OF THE SOCIETY OF ECONOMIC GEOLOGISTS

VOL. 100

November 2005

No. 7

100th Anniversary Special Paper:

Vapor Transport of Metals and the Formation of Magmatic-Hydrothermal Ore Deposits

ANTHONY E. WILLIAMS-JONES[†]

Department of Earth and Planetary Sciences, McGill University, 3450 University Street, Montréal, Québec, Canada H3A 2A7

AND CHRISTOPH A. HEINRICH

Isotope Geochemistry and Mineral Resources, Department of Earth Sciences, Swiss Federal Institute of Technology, ETH Zentrum NO, 8092 Zürich, Switzerland

Abstract

In most published hydrothermal ore deposit models, the main agent of metal transport is an aqueous liquid. However, there is increasing evidence from volcanic vapors, geothermal systems (continental and submarine), vapor-rich fluid inclusions, and experimental studies that the vapor phase may be an important and even dominant ore fluid in some hydrothermal systems. This paper reviews the evidence for the transport of metals by vapor (which we define as an aqueous fluid of any composition with a density lower than its critical density), clarifies some of the thermodynamic controls that may make such transport possible, and suggests a model for the formation of porphyry and epithermal deposits that involves precipitation of the ores from vapor or a vapor-derived fluid.

Analyses of vapor (generally >90% water) released from volcanic fumaroles at temperatures from 500° to over 900°C and near-atmospheric pressure typically yield concentrations of ore metals in the parts per billion to parts per million range. These vapors also commonly deposit appreciable quantities of ore minerals as sublimates. Much higher metal concentrations (from ppm to wt %) are observed in vapor inclusions trapped at pressures of 200 to 1,000 bars in deeper veins at lower temperatures (400°–650°C). Moreover, concentrations of some metals, notably Cu and Au, are commonly higher in vapor inclusions than they are in inclusions of coexisting hypersaline liquid (brine). Experiments designed to determine the concentration of Cu, Sn, Ag, and Au in HCl-bearing water vapor at variable although relatively low pressures (up to 180 bars) partly explain this difference. These experiments show that metal solubility is orders of magnitude higher than predicted by volatility data for water-free systems, and furthermore that it increases sharply with increasing water fugacity and correlates positively with the fugacity of HCl. Thermodynamic analysis shows that metal solubility is greatly enhanced by reaction of the metal with HCl and by hydration, which results in the formation of species such as $\text{MeCl}_m \cdot n\text{H}_2\text{O}$. Nonetheless, the concentrations measured by these experiments are considerably lower than those measured in experiments involving aqueous liquids or determined for vapor fluid inclusions. A possible explanation for this and for the apparent preference of metals such as Cu and Au for the vapor over the coexisting brine in some natural settings is suggested by limited experimental studies of metal partitioning between vapor and brine. These studies show that, whereas Cu, Fe, and Zn all partition strongly into the liquid in chloride-bearing sulfur-free systems, Cu partitions preferentially into the vapor in the presence of significant concentrations of sulfur. We therefore infer that high concentrations of Cu and Au in vapor inclusions reflect the strong preference of sulfur for the vapor phase and the formation of sulfur-bearing metallic gas species.

Phase stability relationships in the system NaCl–H₂O indicate how vapor transport of metals may occur in nature, by showing a range of possible vapor evolution paths for the conditions of porphyry-epithermal systems. At the world-class Bingham Canyon porphyry Cu–Au deposit, evidence from fluid inclusions supports a model in which a single-phase fluid of intermediate to vapor-like density ascends from a magma chamber. On cooling and decompression, this fluid condenses a small fraction of brine by intersecting the two-phase surface on the vapor side of the critical curve, without significantly changing the composition of the expanding vapor. Vapor and brine reach Cu–Fe sulfide saturation as both phases cool below 425°C. Vapor, which is the dominant fluid in terms of the total mass of H₂O, Cu, and probably even Cl, is interpreted to

[†] Corresponding author: e-mail, willyj@eps.mcgill.ca

be the main agent of metal transport. The evolution of fluids leading to high-grade epithermal gold mineralization is initiated by an H_2S -, SO_2 -, Au-, and variably Cu- and As-rich vapor, which separates from an FeCl_2 -rich brine in a subadjacent porphyry environment. In the early stages of the hydrothermal system, vapor expands rapidly and on reaching the epithermal environment, condenses, producing hypogene advanced argillic alteration and residual vuggy quartz and, in some cases, coeval high-sulfidation precious metal mineralization (e.g., Pascua). More commonly, the introduction of precious metals occurs somewhat later, after the site of magmatic fluid exsolution has receded to greater depth. Because of the relatively high pressure, the vapor separating from brine at this stage cools along a pressure-temperature path above the critical curve of the system, causing it to contract to a liquid capable of transporting several parts per million Au to temperatures as low as 150°C .

Introduction

FOR OVER 100 years, interpretations of the genesis of hydrothermal ore deposits, other than those of mercury and sulfur, have concluded that the agent of metal transport is an aqueous liquid. Moreover, this view has prevailed despite evidence that the dominant aqueous phase in several major types of ore-forming hydrothermal systems is commonly vapor. In a benchmark paper, Henley and McNabb (1978) proposed a model for porphyry-type ore deposits in which the metals are transported to the site of deposition by a plume of vapor. However, with a small number of exceptions (e.g., Eastoe, 1982; Sillitoe, 1983), few researchers appear to have considered this model until Heinrich et al. (1992) reported that vapor fluid inclusions in the Mole Granite, Australia, contain greater concentrations of Cu (up to 3 wt % using proton induced X-ray emission (PIXE) analyses) than associated high-salinity liquid inclusions. In the past 5 years, several other studies of fluid inclusions from porphyry-type and other deposits have documented high concentrations of Cu in the vapor phase (e.g., Damman et al., 1996; Heinrich et al., 1999; Ulrich et al. 1999; Baker et al., 2004), and Ulrich et al. (1999) have shown that Au may also partition preferentially into the vapor in this environment.

Part of the reason that metal transport by vapor had not been given much consideration is that thermodynamic studies by Krauskopf (1957, 1964) concluded that the solubility of most metals in aqueous vapor is negligible (Hg, As, and Sb are exceptions), even at temperatures as high as 800°C . However, Krauskopf (1957, 1964) based his estimates on data for the vapor pressure of metallic species over the corresponding solids (i.e., their dry sublimation or volatility) and ignored the possibility that interactions with the solvent might enhance solubility in aqueous vapor. At the time of his studies, there were few experimental data on metal solvation by aqueous vapor at hydrothermal conditions (e.g., Millner and Neugebauer, 1949) and, until recently, such data have been largely restricted to sodium chloride (cf. Martynova, 1964; Pitzer and Pabalan, 1986; Armelini and Tester, 1993). During the past 5 years, however, a number of experimental studies have investigated the stability of metallic species in aqueous vapors and, in each case, have demonstrated that the solubility is orders of magnitude higher than that predicted from volatility data (cf. Williams-Jones et al., 2002). Even at the low temperatures ($\leq 360^\circ\text{C}$) of these experiments, the measured metal concentrations in the vapor phase would be sufficient to permit formation of economic ore deposits and experiments at magmatic conditions (e.g., Simon et al., 2005a, b) have yielded metal concentrations similar to those reported in vapor inclusions from natural systems (cf. Heinrich et al., 1999).

The discovery that the vapor phase is a potentially important medium of metal transport in hydrothermal systems has far-reaching consequences for our interpretation of the formation of a number of intrusion-related ore deposit types and, by extension, for mineral exploration. Until now, the significance attributed to the vapor phase is that boiling causes sharp gradients in physicochemical parameters like temperature, $a_{\text{H}_2\text{S}}$, pH, and f_{O_2} , leading to ore deposition from aqueous liquids (Drummond and Ohmoto, 1985). Indeed, boiling models have been useful guides in gold exploration. If, however, the vapor phase also transports metals to the site of ore deposition, it is important to know how that phase originates, how it dissolves metals, how effectively it sequesters metals relative to the liquid phase, how it evolves as a function of pressure and temperature, and under what conditions it might deposit metallic minerals.

In this paper, we evaluate the role of aqueous vapor as an agent of metal transport during the formation of metallic mineral deposits by examining data currently available from natural systems and experiments. We then use these data to discuss the evolution of upper-crustal magmatic-hydrothermal systems and speculate on how a range of vapor evolution paths might explain the formation of porphyry-style and epithermal ore deposits.

Phase Stability Relationships and Terminology

In pure H_2O fluids, the vapor phase becomes increasingly dense with increasing temperature and pressure along the liquid-vapor curve (boiling curve), whereas the coexisting aqueous liquid expands. At the critical point (374°C , 225 bars), the two phases become indistinguishable, and water exists as a single supercritical fluid (see Table 1 for definitions of terms used to describe fluid phases in this paper). With the addition of salt, the upper limit of two-phase behavior expands to much higher temperatures and pressures, allowing a lower salinity vapor to coexist with a dense high-salinity liquid (a brine) up to at least 2,000 bars and 800°C (Fig. 1A; Sourirajan and Kennedy, 1962; Bodnar et al., 1985; Pitzer and Pabalan, 1986; Bischoff, 1991; Driesner and Heinrich, 2006). These conditions overlap with those of the water-saturated solidus of granitic melts (Burnham, 1979), such that two separate fluid phases may coexist with a hydrous silicate melt in shallow crustal magma chambers (Bodnar et al., 1985; Signorelli and Carroll, 2000), as recorded by coexisting fluid and melt inclusions (Lowenstern, 1994, 1995; Audétat and Pettke, 2003; Fig. 1B).

Based on a review of all available experimental data in the $\text{NaCl-H}_2\text{O}$ system, Driesner and Heinrich (2006) have developed an equation of state linking the properties of low-salinity

TABLE 1. Terminology for Fluid Phases in Saline Hydrothermal Systems

Fluid	Any mobile phase dominated by volatile constituents of the H-O-C-N-S system (e.g., H ₂ O, CO ₂ , SO ₂ , H ₂ S, N ₂) with variable concentrations of dissolved components such as chloride salts
Single-phase fluid	A fluid of any composition and density at a pressure above (or a temperature below) the two-phase (liquid + vapor) surface
Liquid	A water-rich, salt-bearing fluid with a density above the critical density of the corresponding salt-water mixture (e.g., $\rho_{\text{crit}} = 0.32 \text{ g cm}^{-3}$ for pure water; $\rho_{\text{crit}} = 0.48 \text{ g cm}^{-3}$ for 7 wt % NaCl; $\rho_{\text{crit}} = 0.59 \text{ g cm}^{-3}$ for 20 wt % NaCl)
Hypersaline liquid (= brine)	A liquid with >26 wt % NaCl (commonly called "brine;" halite saturated at room temperature)
Aqueous liquid	A dense water-rich (<26 wt % NaCl) liquid at a temperature below the critical point of water (374°C/225 bars) and a pressure at or above the boiling curve of water
Vapor	A water-rich, salt-bearing fluid ($\pm \text{CO}_2$ and other volatiles) with a density below the critical density of the mixture of interest

Notes: Avoidance of the term "supercritical fluid" is recommended because it cannot be clearly defined with reference to pressure and temperature for binary or multicomponent fluid systems; for pure water, supercritical refers to a fluid at pressures and temperatures above its critical point

vapor and high-salinity brine across the critical region. This integrated formulation covers the entire compositional range of stable fluids between pure water and pure NaCl but describes bulk fluid properties without reference to molecular

speciation. A P-T-X diagram from that paper (Fig. 2) shows that the critical curve for the NaCl-H₂O system (i.e., the crest of the limiting two-phase surface, and the highest pressure or lowest temperature at which a separate vapor phase can co-exist with a liquid) is strongly dependent on salinity. Vapor is defined here as any fluid with a density lower than the critical density for the composition of interest (Table 1). At pressures below ~400 bars, a halite- or liquid-saturated vapor will be essentially salt free and have a density below 0.1 g/cm³. However, at ~1,200 bars and ~700°C, for example, the vapor

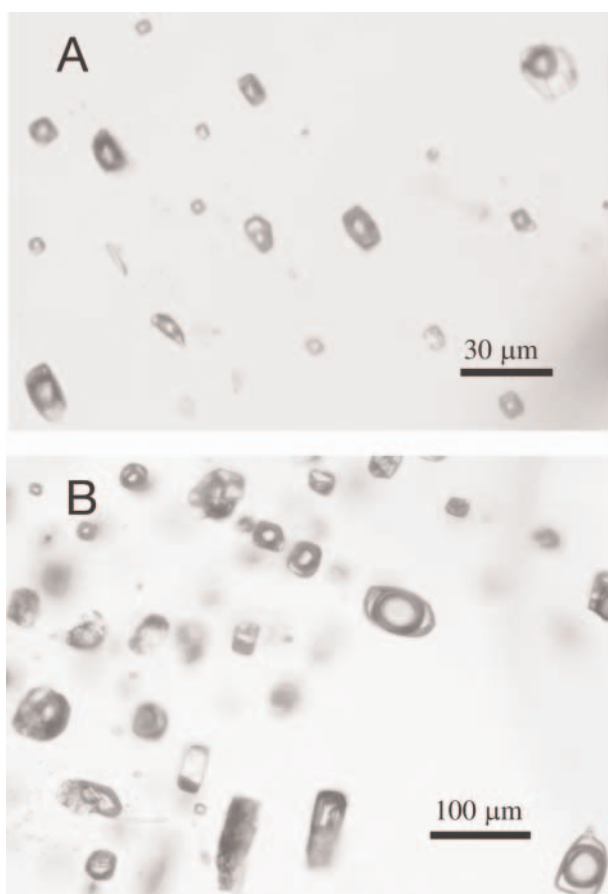


FIG. 1. A. Photomicrograph of hypersaline liquid inclusions trapped on the same healed fracture as numerous vapor inclusions (Questa Mo porphyry deposit, New Mexico). B. Photomicrograph of two large and a few smaller low- to intermediate-density fluid inclusions trapped in the single-phase fluid stability field together with a granitic silicate melt, recorded by numerous crystallized melt inclusions (quartz crystal from a miarolitic cavity in the Rito del Medio Pluton, New Mexico).

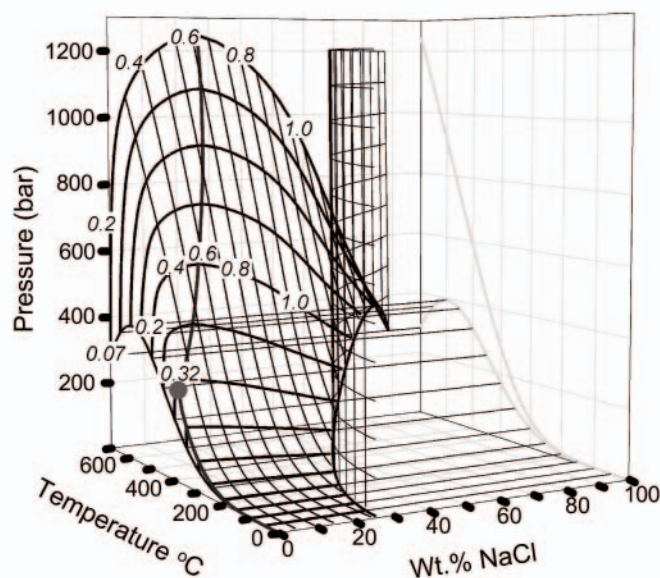


FIG. 2. Perspective representation of phase stability relationships for the binary NaCl-H₂O system in temperature-pressure-salinity space, emphasizing the tunnel-shaped two-phase miscibility surface and the critical curve indicated by the bold crest line. At pressures above this surface, a single-phase fluid of vapor- to liquid-like density is stable, limited toward the right side of the diagram by the solubility of halite (near-vertical saturation surface). Below the gridded miscibility surface, a low-density liquid of low to moderate salinity (left of the critical curve) coexists with a liquid of higher salinity and density (right). At very low pressures but high temperatures, halite coexists with nearly pure water vapor (salinity too low to show in linear scale). Numbers along the two-phase surface denote fluid density in g cm⁻³ (modified from Driesner and Heinrich, 2006).

may contain as much as ~20 wt percent salt and reach a density of ~0.5 g/cm³. No physically defined boundary separates such a vapor from the state commonly referred to as “super-critical” fluid, which is a term we generally avoid here in favor of the less ambiguous term “single-phase fluid.” Depending on the pressure-temperature path followed within the region of single-phase fluid stability, a fluid may expand (decrease its density) or contract (increase its density) and thereby change from a single-phase liquid ($\rho > \rho_{\text{critical}}$) to a single-phase vapor ($\rho < \rho_{\text{critical}}$) or vice versa without crossing a phase boundary. Homogeneous expansion or contraction is clearly distinguished from the processes of boiling and condensation, which describe two modes of phase transition from a single- to a two-phase state (i.e., by separation of vapor bubbles from liquid or liquid droplets from vapor, respectively).

Given the general phase relationships in saline fluid systems, the behavior of minor components, including ore metals, is expected to be sensitive to the highly variable density and chlorinity of the fluids (for a modern introduction to the thermodynamic theory of aqueous fluids at high pressure and temperature see Palmer et al., 2004a). At low density and chlorinity, metal concentrations in the vapor phase are likely to be determined by the dry volatility of the corresponding solids, whereas at higher density and chlorinity, hydration and the formation of complexes become the controlling factors for metal behavior in vaporlike fluids.

Compositions of Volcanic Vapors and Their Sublimates

Volcanic vapors and their sublimates provided the first geologic evidence of the capacity of aqueous vapor to dissolve significant amounts of metals. Analyses of these vapors have also provided important chemical information on how the metals might be transported, suggesting that acidic vapor components could act as ligands in metallic gas species. After H₂O, which typically comprises >90 mol percent of volcanic vapors, the next most important components are CO₂ (up to 10 mol %), SO₂ (up to 6 mol %), and HCl (up to 6 mol %). Other volatiles, of which H₂, HF, and H₂S are the most important, comprise <1 mol percent of the bulk volcanic vapor (Table 2). In principle, any of these volatile components, with the possible exception of H₂, could be involved in the formation of stable metallic species in the vapor phase.

The concentrations of metals in condensed volcanic vapors are highly variable but commonly are on the order of parts per billion and vary with temperature and the composition of the magma (Table 3). For example, condensates of volcanic vapors derived from basaltic magmas commonly have copper concentrations up to several parts per million, whereas those from dacitic or rhyolitic magmas contain parts per billion levels of this metal. Other metals reported as having high concentrations in the vapors emanating from basaltic magmas include Zn, Pb, Sb, As, Ag, and Au. Vapors from andesitic volcanoes yield condensates with concentrations of Cu, Zn, Pb, and As comparable to those of basaltic volcanoes, but substantially higher concentrations of Mo and Hg, up to 3 ppm (Merapi, Indonesia: Symonds et al., 1987) and 340 ppb (Kudryavy, Russia: Taran et al., 1995), respectively. The only metals reported to occur in high concentrations in the condensates of vapors released by rhyolitic and dacitic volcanoes are Sn (e.g., 7 ppm, at Usu, Japan: Giggenbach and Matsuo, 1991) and Mo (e.g., 1 ppm at Satsuma Iwojima, Japan: Hedenquist et al., 1994).

Further insights into the role of the vapor phase in transporting metals can be gleaned from the sublimates (solids precipitated from vapors) forming around volcanic fumaroles (Fig. 3). As early as 1929, Zeiss described high-temperature sublimates in the Valley of Ten Thousand Smokes, United States, containing ilsemanite (Mo₃O₈·nH₂O), sphalerite, chalcocite, covellite, and galena and low-temperature sublimates containing an unidentified orange arsenic sulfide. Since then a large number of other metallic minerals have been reported to form in the sublimates of volcanic vapors, including chalcopyrite, molybdenite, cassiterite, wolframite, scheelite, greenockite, realgar, bismuthinite, and native gold (e.g., Naboko, 1964; Stoiber and Rose, 1974; Symonds et al., 1987; Quisefit et al., 1989; Bernard et al., 1990; Taran et al., 2000).

A number of investigators have induced sublimate formation by inserting meter-long silica tubes into volcanic fumaroles (e.g., Le Guern and Bernard, 1982; Quisefit et al., 1989). This ensures almost complete precipitation in the tube of the metals dissolved in the vapor, as the temperature at the outlet is commonly on the order of 100°C. Moreover, the temperature at which a particular metallic mineral precipitates

TABLE 2. Proportions (wt %) of Major Species in Vapors Discharged by Selected Volcanoes

Volcano	Momotombo ¹	Poas ¹	Mt. Etna ¹	Merapi ¹	Kudriavy ²	Colima ³	Mt. St. Helens ¹	Usu ¹
Magma type	Basalt			Andesite		Dacite		Dacite
Temp (°C)	658–820	960–1045	1075	767–915	605–940	740–820	663–802	656–678
H ₂ O	97.1–97.9	95.28–97.08	22.71–53.69	88.53–95.83	93.1–95.6	89.18–98.7	91.58–98.60	95.80–97.30
H ₂	0.17–0.7	0.39–0.67	0.30–0.57	0.71–1.54	0.24–1.3	0.06–0.63	0.27–0.85	0.27–0.34
CO ₂	1.44–1.47	0.53–1.00	17.08–33.93	3.26–7.56	1.81–2.80	0.8–2.62	0.89–6.94	1.70–3.02
CO	0.002–0.010	0.003–0.01	0.36–0.71	0.02–0.16	0.001–0.23	NA	0.0013–0.06	0.003–0.005
SO ₂	0.3–0.5	1.232–2.004	14.69–47.7	0.06–1.15	1.07–2.33	0.24–2.79	0.067–0.208	0.142–0.258
H ₂ S	0.16–0.29	0.006–0.420	0.12–0.27	0.12–1.16	0.18–0.68	NA	0.099–0.355	0.350–0.714
HCl	2.68–2.89	0.011–0.121	—	0.59	0.09–0.74	0.25–0.51	0.076–0.089	0.024–0.160
HF	0.240–0.259	0.011–0.121	—	0.4	0.013–0.083	0.015–0.051	0.03	0.012–0.033

Notes: NA = not analyzed, — = not detected

¹ Compiled and summarized by Symonds et al. (1994)

² Compiled and summarized by Taran et al. (1995)

³ Compiled and summarized by Taran et al. (2000)

TABLE 3. Concentrations of Metal Species in Fumarole Vapor Condensates from Selected Volcanoes

Volcano	Cerro Negro ¹	Momotombo ¹	Poas ¹	Tobalchik ²	Alkali Basalt	Etna ³	Colima ⁴	Kudriavy ⁵	Merapi ⁶	Mt St Helens ⁷	Usu ⁸	Satsuma Iwo Jima ⁹
Magma type		Basalt						Andesite		Dacite		Rhyolite
Temp (°C)	300–315	456–770	344–852	1010	928	928	738–828	535–940	576–796	710	649	165–877
Hg	0.004–0.005	0.006–0.021	0.01–0.30	–	–	–	NA	0.02–0.34	–	0.02	0.0001	–
As	0.03–0.09	0.23–0.49	–	24	6.1	6.1	0.4–0.5	0.6–1.6	0.28–0.96	1.4	0.02	1.7–4.6
Sb	0.002–0.004	0.003–0.96	0.003–0.008	13	0.02	0.02	0.04–0.13	0.02–0.510	0.16	0.008	0	0.02–0.03
Au	1–2	1–24	–	4	24	24	1.0–5.0	NA	NA	0.03	0.007	0.0015–0.0032
Ag	3–11	5–14	6–250	6	120	120	NA	NA	NA	0.01	0.5	–
Cu	0.2–0.8	0.2–8.4	0.1–0.6	6	–	–	0.4–0.9	0.03–0.91	0.01–1.0	0.05	0.01	0.006–0.064
Pb	NA	1.9–7	0.8–5.4	0.6	12	12	0.08–0.48	0.110–9.7	0.3–1.6	0.5	0.006	0.2–1.8
Zn	0.3–0.6	0.4–7.6	0.5–8.6	9.8	13	13	5–8	0.25–13.5	4–82	0.019	0.04	0.03–0.24
Sn	0.8–1.0	1.1–2.4	1.4–3.9	0.09	–	–	NA	0.1–0.38	–	–	7	0.2–0.8
W	–	–	–	–	–	–	NA	0.002–0.060	0.05–0.13	0.003	0.003	–
Mo	0.18–0.27	0.15–0.5	–	–	–	–	0.09–0.18	0.002–0.270	0.08–2.8	0.094	0.06	0.005–1.07

Notes: All data are reported in ppm, except for gold (ppb); NA = not analyzed, – = not detected
¹ Data from Gemmell (1987)
² Data from Menyailov and Nikitina (1980)
³ Data from Le Guern (1988)
⁴ Data from Taran et al. (2000)
⁵ Data from Taran et al. (1995)
⁶ Data from Symonds et al. (1987)
⁷ Data from Bernard (1985)
⁸ Data from Gigenbach and Matsuo (1991)
⁹ Data from Hedenquist et al. (1994)

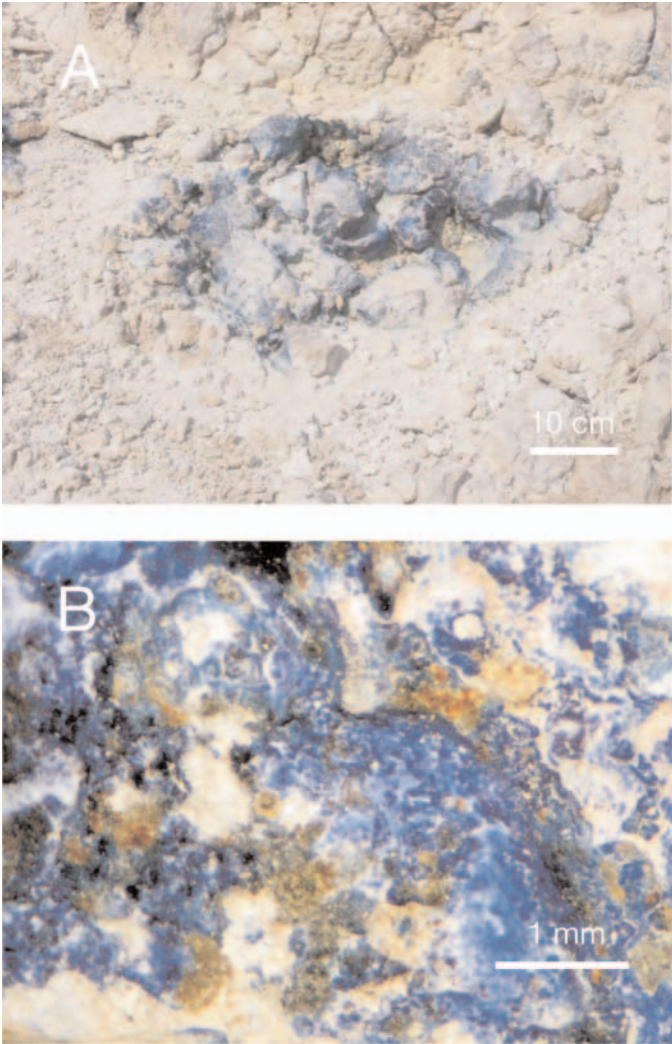


FIG. 3. A. Sublimates around a recently extinct fumarole at the Merapi volcano, Indonesia, displaying the characteristic blue color of the phase, ilsemanite (Mo₃O₈·nH₂O), also known as molybdenum blue. B. A sample of the sublimite shown in (A) viewed under a binocular microscope. The photomicrograph shows characteristic globular coatings of amorphous ilsemanite sublimite on highly altered (kaolinized) andesite.

can be estimated from its location inside the tube. These experiments have shown that magnetite, molybdenite, and wolframite generally precipitate close to the inlet of the tube (i.e., at temperatures >500°C), chalcopyrite, sphalerite, and pyrite commonly precipitate at somewhat lower temperature, and galena, Pb sulfosalts, and native arsenic generally precipitate at temperatures <450°C (Fig. 4). Native gold is rarely observed in silica tube experiments, but Taran et al. (2000) reported its formation at 450° to 550°C in a silica tube experiment at the Colima volcano, Mexico.

An interesting feature of many volcanoes, and particularly well exemplified by the Kudriavy volcano in the Kurile arc, is that there may be several active and relatively closely spaced (separated by <100 m) fumarolic fields depositing distinctly different assemblages of metallic minerals (Korzhinsky et al., 1994; Chaplygin et al., 2005). The main field at Kudriavy (700°–870°C) deposits sublimates of ilsemanite (Mo₃O₈·n

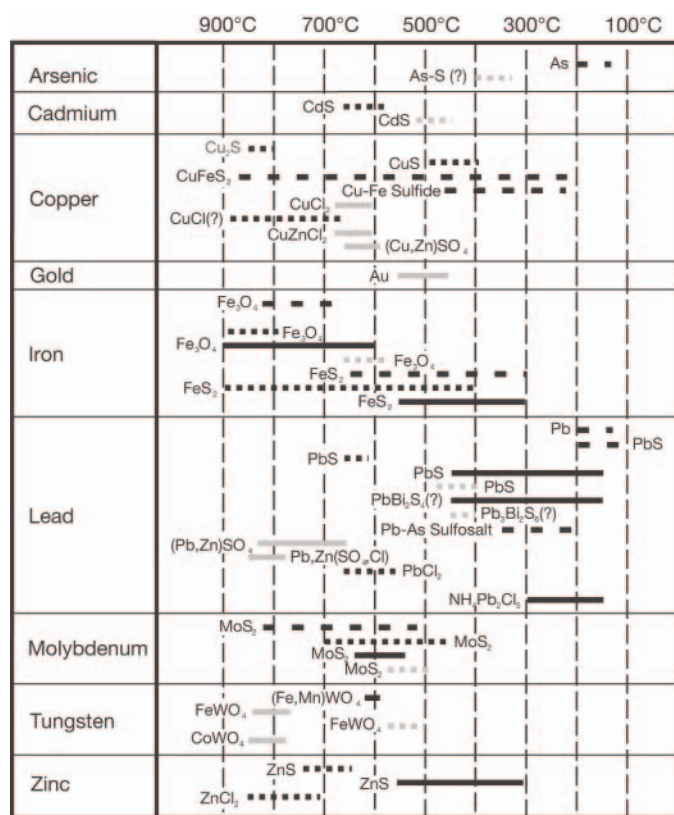


FIG. 4. Temperatures of formation of ore metal-bearing sublimates deposited in silica tubes inserted into high-temperature volcanic fumaroles. The data were taken from Quisefit et al. (1989; Momotombo = dashed black bars), Le Guern and Bernard (1982; Bernard (1985), and Kavalieris (1994; Merapi = solid black bars), Bernard and Le Guern (1986; Mount St. Helens = gray dotted bars), Taran et al. (2000; Colima = gray solid bars), and Wahrenberger et al. (2002; Kudriav = dotted black bars).

H₂O)-molybdenite-molybdenite-magnetite; the dome field (400°–730°C) forms cosalite (Pb₃Bi₂S₅)-lillianite (Pb₃Bi₂S₆)-wurtzite-cadmoindite (CdIn₂S₄); the molybdenum field (400°–650°C) mainly ilsemanite-molybdenite-molybdenite-hematite-magnetite-W-powellite; and the rhenium field (300°–560°C) has greenockite-rhenite (ReS₂)-magnetite as the principal metallic mineral assemblage. Partly, this reflects differences in the saturation temperatures of the different metallic minerals, as indicated by generally lower metal concentrations in vapor condensates of the lower temperature fields. However, contents of Pb, Bi, and Cd are highest in vapor condensates of the dome field, despite the fact that temperatures are lower than in the main field, where minerals of these metals do not deposit (Chaplygin et al., 2005). This suggests that the different pressure-temperature paths traveled by fluids coming ostensibly from the same magmatic source must have influenced the bulk composition of the fluids and, in turn, their metal concentrations.

In summary, data available on the compositions of volcanic vapors and their sublimates provide a clear indication that a variety of common metals can be transported in appreciable concentrations in H₂O-dominated vapors. Moreover, the sublimite data suggest that some metallic minerals (e.g., wolframite and molybdenite) saturate at relatively high temperatures, whereas

others like galena and the sulfosalts have appreciable solubility at quite low temperatures. Finally, volcanic vapor compositions suggest that volatile components like HCl and H₂S are important in enhancing metal solubility through complexation.

Liquid-Vapor Separation in Active Geothermal Systems

Active geothermal systems have been an important source of information for understanding metal transport in the context of hydrothermal ore formation (White, 1956; White et al., 1971; Ellis, 1979; Henley and Ellis, 1983; Giggenbach, 1992). The principal agent of energy transfer in such systems is aqueous liquid of near-neutral pH, but commonly this liquid coexists with vapor. This is confirmed by the presence of vapor and liquid inclusions in rock samples from the deep reservoir of some systems (e.g., Broadlands, New Zealand: Browne et al., 1974; Larderello, Italy: Cathelineau et al., 1994; Mori, Japan: Muramatsu and Komatsu, 1999). There is also semi-quantitative evidence from the composition of the condensed vapor and the nature of the pipe scalings in some geothermal systems that the vapor phase may contribute significantly, and perhaps even dominantly, to the mobilization of some metals (e.g., the rare earth elements, and gold, arsenic, and base metals: Möller et al., 2003; Raymond et al., 2005).

Submarine geothermal systems are dominated by heated seawater and show very different phase behavior to those on land because they are located under several kilometers of water. As a result of the higher fluid pressure, black smokers at mid-ocean ridges usually expel a single-phase fluid. Nevertheless, significant deviations from seawater salinity and even highly transient salinity fluctuations do occur in some systems (Von Damm et al., 1997, 2003). These are best explained by liquid-vapor separation in the subsurface, which is consistent with the coexistence of liquid and vapor fluid inclusions in samples recovered from gabbroic rocks exposed at sea-floor faults or from ophiolites (e.g., Kelley et al., 1992; Vanko et al., 2004). Phase separation recorded by black smoker effluents occurs at conditions close to the critical point of seawater (407°C and 298 bars), leading to two fluids that differ only moderately in their total salinity (Fig. 2), with chloride contents ranging from about one-tenth (vapor) to twice seawater salinity (residual liquid: Von Damm et al., 1997). End-member vapor and liquid phases, differing in chlorinity by a factor of 1.9, were sampled separately from the Brandon vent on the East Pacific Rise (Von Damm et al., 2003). The vapor phase is typically enriched in volatiles including CO₂, H₂S, and B(OH)₃ (Von Damm et al., 1997; Seyfried et al., 2003), but metal concentrations (e.g., Cu and Zn) are proportional to chloride concentrations, and metal ratios are not measurably different in liquid and vapor phases (Von Damm et al., 2003). This similarity in the behavior of the base metals in the two fluids is consistent with their strong complexation by chloride ions (Barrett and Anderson, 1987; Xiao et al., 1998) and the relatively small differences in the density and salinity of the two fluids due to their separation at near-critical conditions (Palmer et al., 2004b). The data from black smokers thus show that ore metals are relatively soluble in the dense vapor phase of boiling submarine hydrothermal systems, reaching ~100 μmol/kg for base metals like Cu and Zn that may become enriched in volcanogenic massive sulfide deposits (Von Damm et al., 2003).

Metal-Rich Vapor Inclusions in Ore Deposits and Intrusions

High-temperature volcanic vapor, low-density vapor in continental geothermal systems, and relatively dense vapor derived from near-critical boiling of seawater in submarine hydrothermal vents all indicate a significant capacity of water-rich vapor to transport metals. Ore metal concentrations greatly exceed those expected from the volatility of dry metal salts. One may therefore expect that dense water vapor at elevated pressures and temperatures will be able to dissolve even higher concentrations of metals. Fluid inclusions trapped in magmatic-hydrothermal ore deposits and associated upper crustal intrusions confirm this expectation. Moreover, they show that the separation of a lower salinity vapor phase from a dense hypersaline liquid (Fig. 1) may lead to significant fractionation of metals and selective enrichment of ore-forming components.

Natural vapor-brine inclusion assemblages

The first evidence that magmatic vapors can have very high concentrations of copper, at wt percent levels rather than in the parts per million range reported for volcanic vapors, came from estimates of the size of chalcopyrite daughter crystals in vapor inclusions of porphyry copper deposits (Fig. 5; Roedder, 1971; Eastoe 1978) and from Cu-rich vesicles in silicic lavas (Lowenstern et al., 1991). Etminan (1977) and Sawkins and Scherckenbach (1981) used the size of daughter crystals to show that copper concentrations in vapor inclusions can be higher than those in associated brine inclusions. These observations were supported by experimental data showing high solubility of metals in the vapor phase (unpublished data; R.W. Henley, pers. commun.), which helped inspire the magmatic vapor plume model (Henley and McNabb, 1978), and in turn prompted the thermodynamic analysis of the vapor transport of metals by Eastoe (1978, 1982). However, the role of vapor as a medium of metal transport in ore-forming hydrothermal systems remained largely ignored until the advent of microanalytical techniques employing PIXE, synchrotron X-ray fluorescence (SXRF), and laser ablation induced coupled plasma mass spectrometry (LA-ICPMS) for quantitative fluid inclusion analysis.

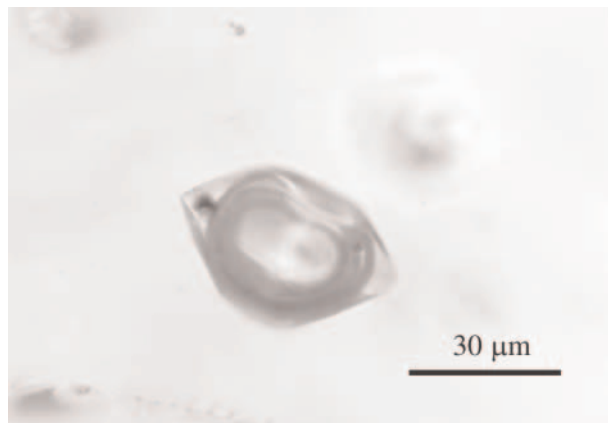


FIG. 5. A single vapor inclusion with a clearly visible triangular chalcopyrite crystal in ore-stage vein quartz from the Granisle porphyry copper deposit, British Columbia.

Analyses using the new techniques showed that even low-density and virtually salt-free vapor inclusions trapped below the critical point of water can have ore-metal concentrations in the 1 to 10 ppm range (e.g., preore fluids in the Madan Pb-Zn veins, Bulgaria; Heinrich et al., 1999; Kostova et al., 2004) and that very much higher metal contents, in the wt percent range, are possible in vapor inclusions coexisting with brine at higher temperatures and pressures (Appendix). Element-specific behavior in brine and vapor inclusions was first quantified in quartz-cassiterite veins from the Mole Granite, Australia (Heinrich et al., 1992), but unusually high Cu contents were subsequently observed in vapor inclusions from the porphyry copper deposits of Bingham Canyon, Utah (Bodnar, 1995) and Rosia Poeni, Romania (Damman et al., 1996), in a Pb-Zn-rich skarn deposit in Mexico (Baker et al., 2004), and in carbonic vapor inclusions coexisting with brines in Cu-Au-PGE-rich veins in the footwall of the Sudbury igneous complex (Hanley et al., 2005). Laser ablation ICPMS instruments with good petrographic control allowed quantitative microanalysis of single brine and vapor inclusions trapped simultaneously along healed fractures ("boiling trails"). Results showed that significant and element-specific fractionation between saline liquids and vapor is widespread in magmatic-hydrothermal settings and across a range of pressures (200–800 bars) and temperatures (350°–700°C; Audétat et al., 1998, 2000; Heinrich et al., 1999; Ulrich et al., 2001; Audétat and Pettker, 2003; Kehayov et al., 2003; Landtwing et al., 2005).

Figure 6 shows a summary of published data on the apparent equilibrium distribution of selected elements between texturally coexisting brine and vapor inclusions trapped in natural quartz samples at temperatures between 350° and 700°C and pressures between 200 and 800 bars. The data are expressed in terms of element distribution coefficients between the two fluid phases by normalizing each element to Na in order to approximate a thermodynamic exchange equilibrium constant and to reduce the effects of total salinity upon brine/vapor fractionation:

$$K_d = \frac{C_{Me}^V}{C_{Na}^V} \frac{C_{Na}^L}{C_{Me}^L}, \quad (1)$$

where C refers to the concentration (in wt units) of the subscripted metal (Me, Na) in either of the phases, vapor (V) or brine (L). This empirical fractionation constant is analogous to that used by Candela (1989a) to describe experimental fluid/melt equilibrium partitioning and provides a measure of the preference of an element for the vapor relative to the dominant cation, Na^+ . The data show that elements like K, Mn, and Fe, and possibly Rb and Cs, prefer the brine slightly over the vapor, and other elements including Zn, Tl, and Pb have no systematic preference. By contrast, B, Cu, As, Sb, and Au, and possibly Li partition in favor of the vapor phase, relative to Na. The magnitude of this fractionation into the vapor varies significantly from sample to sample, particularly for Cu. Based on the available data, the value of K_d shows no simple correlation with total brine salinity or with the physical conditions (pressure-temperature) of entrapment, even though it is clear that the fractionation constant must become unity where pressure-temperature conditions approach the crest of the two-phase surface, such that liquid and vapor become physically indistinguishable (Fig. 2). The lack of a cor-

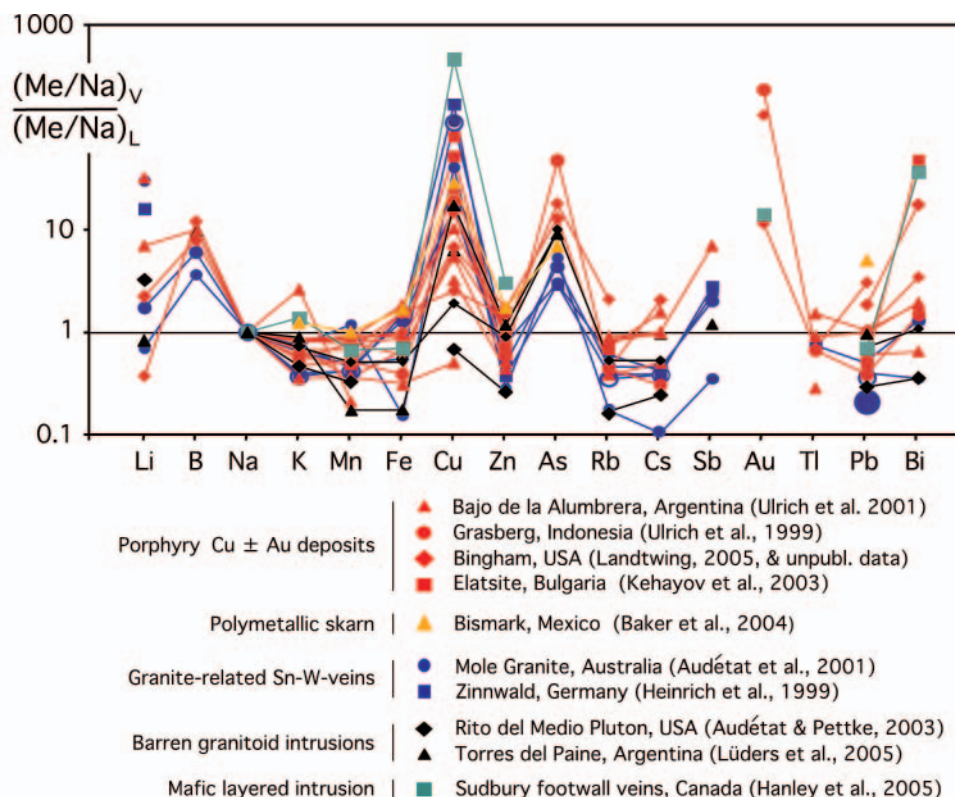


FIG. 6. A summary of microanalytical data from natural assemblages of texturally coexisting but separately trapped vapor (V) and liquid (brine, B) inclusions in high-temperature magmatic-hydrothermal ore deposits and miarolitic cavities of barren granites. The relative preference of each element for the vapor phase in each sample is shown, normalized to the behavior of Na according to equation (1) in the text. Elements such as B, As, and Cu, consistently plotting above $K_d = 1$, fractionate preferentially into the vapor phase relative to Na, which together with most other chloride-complexed cations is enriched in the liquid phase in absolute concentration terms (data from Heinrich et al., 1999, and other sources indicated in the legend). Data from Baker et al. (2004) for Na concentration in vapor was estimated from the average Na/K ratio in all other vapor analyses.

relation of K_d with pressure and temperature is an indication that chemical factors (i.e., hydration and complex formation) rather than purely physical parameters (e.g., fluid density) exert the first-order influence on the highly selective brine-vapor partitioning of different metals.

Single-phase magmatic fluids

Single-phase fluids separating from hydrous magmas have commonly been referred to as the “magmatic vapor phase” (Candela, 1989b), in recognition of the fact that they typically have moderately low salinity and density, comparable to those of many fluids that coexist as a distinct vapor phase with a more saline liquid. Rusk et al. (2004) showed that early porphyry Cu-Mo stockwork mineralization and spatially related sericite alteration at Butte, Montana, were caused by a single-phase fluid of relatively low salinity (~4 wt % NaCl equiv) and intermediate density (~0.6 g cm⁻³). Prior to chalcopyrite and pyrite saturation, this fluid contained very high copper concentrations, on the order of 1 wt percent. Even though this ore fluid would be a liquid according to our definition (Table 1), it has a composition similar to that of lower density vapor inclusions at Grasberg, rather than that of coexisting inclusions of hypersaline liquid (Ulrich et al., 1999; see table 3 in Heinrich, 2005).

In a recent study of the Bingham Canyon deposit, Redmond et al. (2004) and Landtwing et al. (2005) found a vertical transition from single-phase fluid inclusions with a density slightly below the critical density in the deep feeder intrusion, to a two-phase fluid association of brine and vapor inclusions in the high-grade porphyry Cu-Au-Mo orebody. This internally zoned orebody has a conspicuously sharp base in terms of copper and gold grades, which lies 300 to 400 m above the transition from the deep single-phase fluid to the overlying two-phase fluid regime, as recorded by the distribution of inclusion assemblages (Fig. 7). The salinities of the deep (intermediate-density) and the shallower vapor inclusions cannot be determined unambiguously from microthermometry because of the presence of significant CO₂ in these fluids. However, their microthermometric behavior and element ratios, as determined by LA-ICPMS analyses, are almost indistinguishable, and both fluids were very Cu rich prior to saturation with Cu-Fe sulfides ($0.2 < \text{Cu/Na} < \sim 1$; Landtwing et al., 2005).

Brine and Vapor Metal-Partitioning Experiments

Further insights into the capacity of the vapor phase to transport ore metals have been provided by a small number of experiments designed to measure the partitioning of elements among silicate melt, brine, and vapor (e.g., Williams et

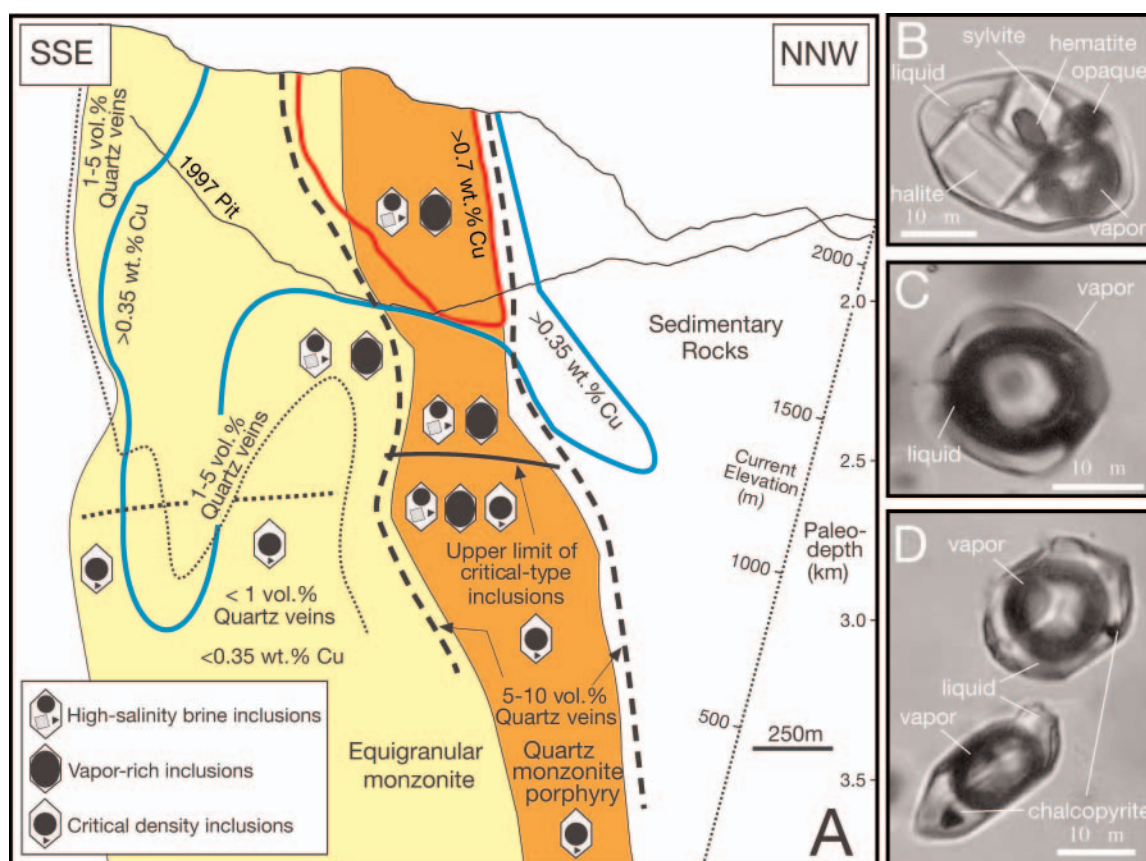


FIG. 7. A. A cross section through the Bingham orebody, showing the distribution of high-salinity brine inclusions, vapor inclusions, and inclusions with near-critical density (modified after Redmond et al., 2004, and Landtwing et al., 2005). Also shown are the distribution of quartz veins and contours representing >0.35 and >0.7 wt percent Cu grades. As is evident from this figure, the fluid evolved from a single phase with near-critical density to a two-phase association of brine and vapor. The orebody has a conspicuously sharp base defined by a sharp drop in copper and gold grades; this base lies well above the transition from the deep single-phase to the overlying two-phase fluid regime. B. Multisolid-bearing brine inclusion. C. Vapor fluid inclusion. D. Coexisting chalcopyrite-bearing vapor and near-critical density fluid inclusions.

al., 1995; Schatz et al., 2004; Simon et al., 2005a-c) or simply between the two aqueous phases (e.g., Shmulovich et al., 2002; Nagaseki and Hayashi, 2004; Pokrovski, 2004; Pokrovski et al., 2005; see Palmer et al., 2004b for the thermodynamic theory of vapor-liquid element partitioning). In the first such experiments involving ore metals, Williams et al. (1995) investigated the partitioning of copper among high-silica rhyolite melt (Bishops Tuff glass), brine, and vapor in rapid-quench, cold-seal vessels at temperatures of 800° and 850°C and pressures of 1,000 and 500 bars, respectively; oxygen fugacity was controlled to two log units above the nickel-nickel oxide buffer (NNO). Although the experimental method did not allow for direct measurement of the concentration of copper in the two aqueous phases, it was possible to evaluate the partitioning of copper between these phases by plotting the apparent equilibrium constants for copper-sodium exchange among melt, brine, and vapor given by the expression

$$K_{\text{Cu,Na}}^{\text{aqm/mlt}} = \frac{C_{\text{Cu}}^{\text{aqm}}}{C_{\text{Cu}}^{\text{mlt}}} \frac{C_{\text{Na}}^{\text{mlt}}}{C_{\text{Na}}^{\text{aqm}}}, \quad (2)$$

where C refers to concentration, aqm is the aqueous mixture at room temperature, and mlt is silicate melt (Candela, 1989a) against ΣCl . In the two fluid phase region, the

composition of brine and vapor is fixed, and thus a change in ΣCl simply indicates a change in the proportions of the two phases. Thus, if the two components (Cu and Na) have the same brine-vapor partition coefficients, the value of the equilibrium constant will not change with ΣCl .

The results of the above experiments showed that $K_{\text{Cu,Na}}^{\text{aqm/mlt}}$ does not vary systematically over a range of chloride concentrations between approximately 0.1 and 3.7 m , indicating that the partitioning of Cu between the two phases is similar to that of Na (i.e., that, in this chemical system, Cu partitions strongly into the brine). Actual distributions for Cu between brine and vapor ($D_{\text{Cu}}^{\text{brine/vap}}$) were determined by assuming that $C_{\text{Cu}}^{\text{vap}}$ was given by $C_{\text{Cu}}^{\text{aqm}}$ for experiments conducted at conditions just outside the low-salinity limb of the solvus (~20 ppm at 850°C and 500 bars and ~120 ppm at 800°C and 1,000 bars), and then evaluating $C_{\text{Cu}}^{\text{brine}}$ from the total chlorinity and $C_{\text{Cu}}^{\text{aqm}}$ for experiments conducted in the two-phase region. Based on this modeling, Williams et al. (1995) reported values for $D_{\text{Cu}}^{\text{brine/vap}}$ ($C_{\text{Cu}}^{\text{brine}}/C_{\text{Cu}}^{\text{vap}}$) of 200 at 850°C and 500 bars and 120 at 800°C and 1,000 bars, suggesting that the partition coefficient increases with increasing temperature and/or decreasing pressure or vapor density. The results of these experiments, however, do not explain the findings of fluid

inclusion studies, which indicate that copper partitions preferentially into the vapor phase.

More recently, Simon et al. (2005a-b) used LA-ICPMS analyses to measure the solubility of iron and gold in synthetic vapor and brine fluid inclusions trapped from an assemblage of vapor + brine + haplogranite + magnetite + gold metal. The experiments were conducted in cold-seal pressure vessels at 800°C and pressures varying from 1,100 to 1,450 bars; oxygen fugacity was controlled by the NNO buffer. The results of the study show that vapor containing from 2.3 to 19 wt percent NaCl equiv coexisted with brine ranging in composition from 57 to 35 wt percent NaCl equiv, respectively. The concentrations of Fe in vapor and brine decreased from 4.1 to 0.3 and 7.2 to 6.4 wt percent, respectively, as pressure decreased from 1,450 to 1,100 bars (Table 4). The corresponding partition coefficients, $D_{Fe}^{vap/brine}$ ranged from 0.56 to 0.05, respectively. The data indicate that iron is concentrated in both brine and vapor but that the brine is preferred. Gold concentrations in the vapor decreased from 36 to 5 ppm, and in the brine from 50 to 28 ppm, as pressure decreased from 1,450 to 1,100 bars, i.e., partitioning of gold between vapor and brine was subequal at the higher pressure, close to the critical pressure (Fig. 8), but brine was strongly favored at the lower pressure (Table 4).

Pokrovski et al. (2004, 2005) determined liquid-vapor partition coefficients for Ag, As, Au, Cu, Fe, Sb, and Zn in the system $H_2O-NaCl \pm HCl$ at temperatures between 350° and 450°C using rigid Ti alloy and flexible-cell reactors, both of which allow sampling of the vapor and liquid during the experiment. The results of these experiments showed that in all cases the metals partitioned into the liquid but that the preference for liquid was strongest for Fe, Cu, Zn, and Ag (i.e., metals that are known to form strong complexes with chloride ions in the liquid phase; Fig. 9). In the case of Cu (and Fe), the results also confirmed the finding of Williams et al. (1995) that the partition coefficients for this metal are similar to those for Na. Vapor/liquid partition coefficients were significantly higher for Au and Sb and, as might be expected from its very high volatility, were highest for As. Significantly, the partition coefficients for As and Sb predict the degree of preference of these elements for the vapor phase reasonably well, as determined by analyses of natural brine plus vapor inclusion pairs (Fig. 6). By contrast, experiments in the Cu-Cl-O-H system failed to explain the preference of Cu for the vapor in some natural systems, which seems to be at variance with the suggestion of Mavrogenes et al. (2002) that Cu is volatilized as a simple hydroxy complex and probably implies that ligands other than Cl serve to enhance the solubility of Cu in natural vapors.

Nagaseki and Hayashi (2004) conducted a preliminary experimental study of the partitioning of Cu and Zn between

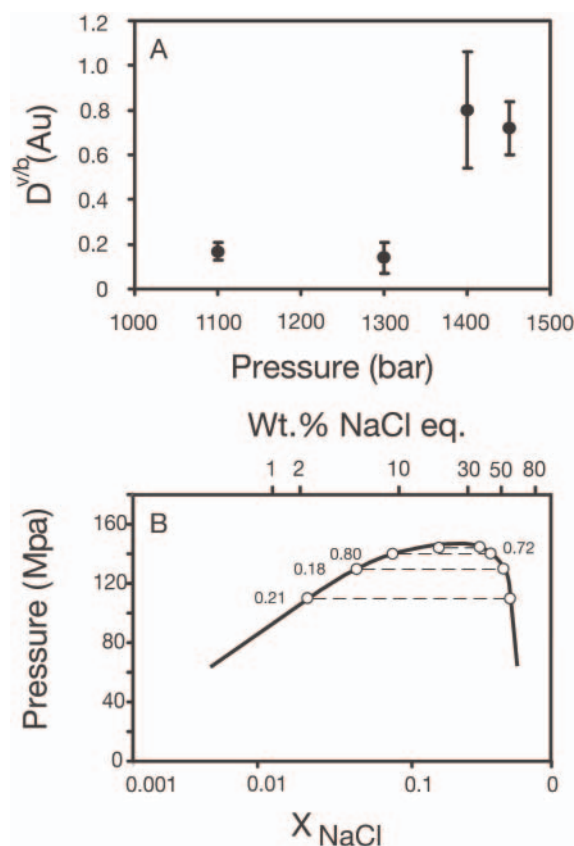


FIG. 8. A. Experimentally determined partition coefficients from Simon et al. (2005a) for the fractionation of gold between coexisting vapor and brine ($\text{NaCl-H}_2\text{O}$) as a function of pressure at 800°C and oxygen fugacity buffered at NNO. B. Distribution of the partition coefficients in (A) as a function of pressure and X_{NaCl} . Also shown is the solvus for the system $\text{NaCl-H}_2\text{O}$.

vapor and liquid at temperatures between 400° and 600°C and pressures between 200 and 500 bars in an $\text{NaCl-H}_2\text{O}$ system containing variable amounts of sulfur. The experimental method involved trapping the fluids as inclusions in quartz and analyzing them using synchrotron X-ray fluorescence. The starting solutions contained HCl, 10 to 30 wt percent NaCl, and had total concentrations of Cu and Zn ranging from 1,000 to 12,000 ppm. Sulfur was added in elemental form as a powder, generating a relatively oxidized sulfur-rich environment. Analyses showed that vapor inclusions from the sulfur-free experiments contained negligible Cu and Zn. By contrast, vapor inclusions from the experiments in which sulfur powder was added to the solutions (1.4–1.7 mol/kg) contained about 3,000 ppm Cu and 100 ppm Zn, whereas the

TABLE 4. Partition Coefficients ($\pm 2\sigma$) for Iron and Gold between Coexisting Vapor and Brine at 800°C and Variable Pressures (Simon et al., 2005 a-b)

P (bar)	Wt % NaCl	Wt % NaCl	Vapor	Fe $\mu\text{g/g}$ ($\pm 2\sigma$)	$D^{v/b}$	Vapor	Au $\mu\text{g/g}$ ($\pm 2\sigma$)	$D^{v/b}$
	equiv Vapor	equiv Brine						
1100	2.1–2.4	56–58	$3.1 \pm 0.74 \times 10^3$	$6.4 \pm 0.6 \times 10^3$	0.05 ± 0.01	5 ± 2	29 ± 4	0.17 ± 0.04
1300	4.9–5.3	50–53	$1.0 \pm 0.26 \times 10^4$	$7.2 \pm 2.0 \times 10^3$	0.14 ± 0.04	4 ± 1	28 ± 4	0.14 ± 0.07
1400	8.8–9.3	42–44	$2.0 \pm 0.2 \times 10^4$	$7.3 \pm 0.8 \times 10^3$	0.27 ± 0.04	28 ± 8	40 ± 10	0.80 ± 0.26
1450	18.7–19.2	35–37	$4.1 \pm 0.77 \times 10^4$	$7.2 \pm 1.6 \times 10^3$	0.56 ± 0.01	36 ± 11	50 ± 7	0.72 ± 0.12

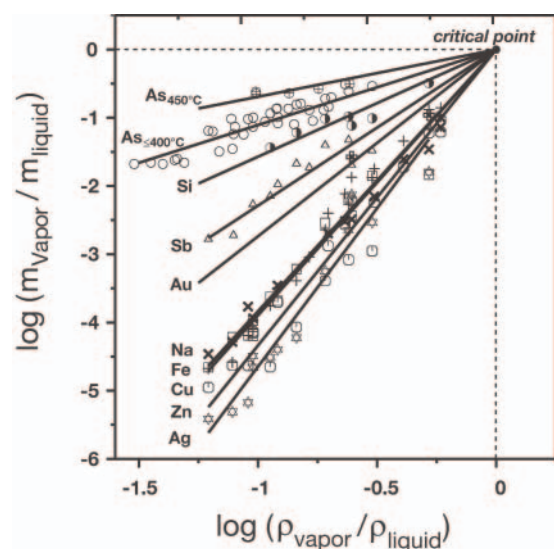


FIG. 9. A ray diagram from Pokrovski et al. (2005), showing apparent vapor/liquid partition coefficients of a number of elements as a function of the density ratio of the two phases, based on experimental data for temperatures between 350° and 450°C. The symbols represent experimental data for the different elements: (○) = As(III) at <400°C, (⊕) = As(III) at 450°C (●) = Si, (Δ) = Sb(III), (◐) = Au(I), (+) = Na, (✕) = Fe(II), (□) = Cu(I), (◑) = Zn, (⊞) = Ag(I).

coexisting brine inclusions contained 100 ppm Cu and 3,000 to 4,000 ppm Zn. These results and recent data reported by Simon et al. (2005c) support the suggestion that high concentrations of sulfur, possibly as HS^- or, given the high f_{O_2} of porphyry and high-sulfidation epithermal systems, SO_3^{2-} , are responsible for preferential stabilization of Cu and Au in the vapor phase.

Experimental Studies of Metal Solubility in Water Vapor

Lessons from the system NaCl-H₂O

In order to be able to successfully model the solubility of metals in water vapor at hydrothermal temperatures, we need experimental data on appropriate H₂O vapor solutions involving metals and ligands analogous to those for aqueous liquid solutions (cf. Seward and Barnes, 1997). As discussed above, such data are extremely limited, and until the late 1990s were restricted to alkali metal chlorides. The system that has been studied most extensively by experimentalists is NaCl-H₂O (Sourirajan and Kenedy, 1962; Martynova, 1964; Styrikovich, 1969; Galobardes et al., 1981; Bischoff et al., 1986; Armellini and Tester, 1993), which provides a valuable template for studies of reactions involving other very weakly volatile metals and H₂O-bearing gas mixtures.

The sublimation of crystalline NaCl (halite) can be described by the following reaction:



The thermodynamic properties of both phases are well known (e.g., Pankratz, 1982, 1984), and thus the equilibrium constant of this reaction and the partial pressure of NaCl^{gas} can be calculated for any temperature that might be of interest in modeling metal transport in ore-forming hydrothermal systems. If NaCl^{gas} were to behave ideally, its solubility in

water vapor could be calculated from its partial pressure and the total vapor pressure in the H₂O-NaCl system ($C_{\text{NaCl}^{\text{gas}}} = \frac{P_{\text{NaCl}^{\text{gas}}}}{P_{\text{total}}}$). However, the experimental studies mentioned above have clearly demonstrated that dissolution of NaCl in water vapor is highly nonideal under hydrothermal conditions, and that the experimentally measured solubilities and those calculated using the Ideal Gas Law can differ by many orders of magnitude.

One way of dealing with this nonideality is to distinguish between a simple reactant gas species and a mixed product gas species. Thus, experimentalists have shown that the equilibrium between NaCl^{gas} and the mixed gas species can be described by a solvation reaction of the type:



This approach offers an important advantage over other approaches (e.g., using equations of state) in that the fugacity of the mixed gas (NaCl-H₂O) can be predicted to a first approximation by the Lewis-Randall rule for ideal mixtures of non-ideal gases (e.g., Galobardes et al., 1981; Armellini and Tester, 1993) and therefore can be applied to complex systems such as those found in nature.

Experimental approach

As has already been mentioned, the volatility of most ore metals (their vapor pressure over the corresponding solids) is extremely low, and thus like NaCl, which also has very low volatility, their behavior in water vapor will be highly nonideal at elevated temperatures. However, as for NaCl, their solubility in water vapor can be modeled using the Lewis-Randall rule for ideal mixtures of nonideal gases. This rule states that the fugacity of the mixed gas is the sum of the products of the partial pressures and fugacity coefficients of the individual gases in the mixture. Consequently, if the fugacities of metallic gas species in pure gases or simple binary gas systems can be determined experimentally (e.g., H₂O-HCl-MeX or H₂O-H₂S-MeX, where Me refers to the metal and X the ligand), their corresponding fugacities in more complex gas systems can be predicted by adding the products of their partial pressures and fugacity coefficients in the simple systems. Using this approach, Williams-Jones and coworkers have begun conducting experiments aimed at measuring the solubility of selected metals and metallic compounds in pure gases (e.g., H₂S and H₂O or simple binary gas systems such as HCl-H₂O) in the hope of eventually using these data to predict their behavior in more complex systems (e.g., Migdisov et al., 1999; Archibald et al., 2001, 2002; Zakaznova-Iakovleva et al., 2001; Migdisov and Williams-Jones, 2005; Rempel et al., 2005). An important finding discussed below is that the species identified to date in these experiments have the form $\text{MeX} \cdot (\text{H}_2\text{O})_n$ or $\text{MeX} \cdot (\text{H}_2\text{S})_n$. Therefore they represent solute molecules or inner sphere complexes surrounded by solvation shells (hydration shells in the case of H₂O), where the subscript “n” is simply a statistical value indicating the average number of solvent molecules surrounding the solute molecule (Fig. 10).

The experiments were carried out in autoclaves constructed from titanium alloy and loaded with a known mass of liquid and preweighed quartz holders containing ampoules with the solid of interest; the ampoules are open at the top but are



FIG. 10. A sketch illustrating the statistical nature of hydration shells (large dashed open circles) forming around molecules of an inner sphere complex (MeCl) indicated by the dark solid circles. The upper molecule is surrounded by four water molecules, whereas the lower molecule only has two water molecules in close proximity. Based on this diagram, the average number of water molecules surrounding molecules of the inner sphere complex (MeCl) is three and thus the statistical hydration number of the species is three.

isolated from the liquid at ambient temperature. At the conditions of the experiment, the liquid is converted entirely to vapor, which fills the autoclave and reacts with the solid in the holder. After an experiment, the autoclave is aircooled to room temperature, and the condensates collected for analysis.

Metal speciation

In order to test for solvation and the formation of inner-sphere Me-Cl complexes, experiments were conducted for a range of $P_{\text{H}_2\text{O}}$ at fixed P_{HCl} and vice versa. Results of these experiments show that, in all cases, the solubility of the metal or metallic compound, and thus its mole fraction in the vapor phase, increased significantly with increasing $P_{\text{H}_2\text{O}}$, providing clear evidence that solvation (hydration) enhanced solubility (Fig. 11A). If hydration had not played a role in dissolving the metal or metallic compound, the vapor pressure of the metallic species would have remained constant, and its mole fraction in the vapor phase would have decreased with increasing $P_{\text{H}_2\text{O}}$. Solubility also increased with increasing P_{HCl} except for experiments that investigated the solubility of silver and copper, which were conducted with AgCl and CuCl. In these latter cases, the solubility was independent of P_{HCl} (Fig. 11B). These results show that solubility was enhanced by the formation of inner sphere Me-Cl complexes and that, in the case of Ag and Cu, the species has a 1/1 Me/Cl ratio. This does not

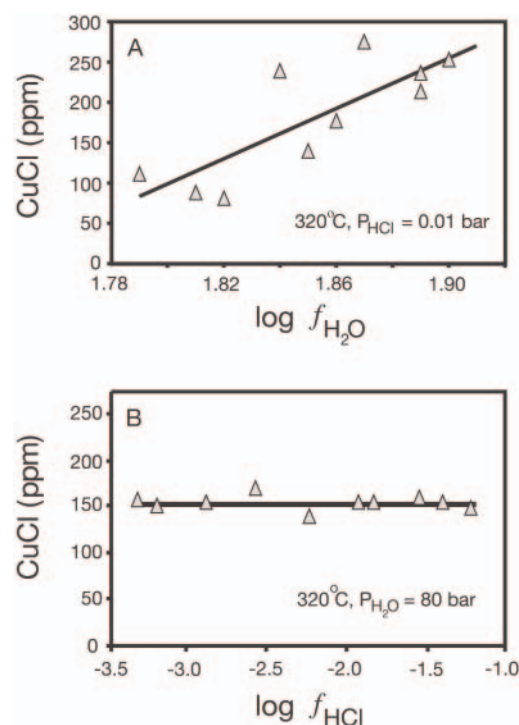
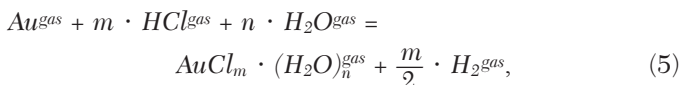


FIG. 11. A. Plot of the concentration of CuCl in the vapor phase as a function of $\log f_{\text{H}_2\text{O}}$ at constant f_{HCl} (modified after Archibald et al., 2002). The increase in CuCl concentration with increasing $f_{\text{H}_2\text{O}}$ indicates that copper solubility was enhanced by hydration. B. Plot of the concentration of CuCl as a function of $\log f_{\text{HCl}}$ at constant $f_{\text{H}_2\text{O}}$. The independence of CuCl concentration from $\log f_{\text{HCl}}$ indicates the formation of an inner sphere complex involving Cu and Cl in the ratio 1/1.

necessarily mean a stoichiometry of MeCl, although this was interpreted to be the case for Ag, as the dominant species in the H_2O -free vapor system has been shown to be AgCl (Tagirov et al., 1993; Hildenbrand and Lau, 1996). The dominant vapor species in the system Cu-Cl are Cu_3Cl_3 and Cu_4Cl_4 (Peterson, 1973; Krabbes and Oppermann, 1977). Based on this and a relatively high hydration number (see below), it was concluded that the inner sphere complex in the copper experiments most likely had the stoichiometry Cu_3Cl_3 (Archibald et al., 2002).

Where the solid dissolved was not a chloride, the nature and stoichiometry of the inner sphere complexes were interpreted by postulating reactions for their formation and corresponding expressions for their equilibrium constants. Thus, in the case of gold, which was introduced as the native metal, the proposed reaction is:



and the expression for the equilibrium constant:

$$\log K_f = \log f_{\text{AuCl}_m \cdot (\text{H}_2\text{O})_n} + \frac{m}{2} \cdot \log f_{\text{H}_2} - n \cdot \log f_{\text{H}_2\text{O}} - m \cdot \log f_{\text{HCl}} - \log f_{\text{Au}}. \quad (6)$$

If $\log K_f$ is differentiated with respect to $\log f_{\text{HCl}}$, while holding temperature, f_{O_2} and $f_{\text{H}_2\text{O}}$ constant, and if the equilibrium

constant of a homogeneous gaseous reaction is independent of total pressure, equation (6) becomes:

$$\left(\frac{\partial \log K_f}{\partial \log f_{\text{HCl}}} \right)_{T, f_{\text{H}_2\text{O}}, f_{\text{O}_2}} = 0 = \left(\frac{\partial \log f_{\text{AuCl}_m(\text{H}_2\text{O})_n}}{\partial \log f_{\text{HCl}}} \right)_{T, f_{\text{H}_2\text{O}}, f_{\text{O}_2}} + \frac{m}{2} \cdot \left(\frac{\partial \log f_{\text{H}_2}}{\partial \log f_{\text{HCl}}} \right)_{T, f_{\text{H}_2\text{O}}, f_{\text{O}_2}} - m \cdot \left(\frac{\partial \log f_{\text{HCl}}}{\partial \log f_{\text{HCl}}} \right)_{T, f_{\text{H}_2\text{O}}, f_{\text{O}_2}} + \left(\frac{\partial \log f_{\text{Au}}}{\partial \log f_{\text{HCl}}} \right)_{T, f_{\text{H}_2\text{O}}, f_{\text{O}_2}} \quad (7)$$

If it is further assumed that f_{H_2} is constant, at constant $f_{\text{H}_2\text{O}}$ and f_{O_2} , and that the dependence of f_{Au} on f_{HCl} is negligible, equation (7) simplifies to:

$$\left(\frac{\partial \log f_{\text{AuCl}_m(\text{H}_2\text{O})_n}}{\partial \log f_{\text{HCl}}} \right)_{T, f_{\text{O}_2}, f_{\text{H}_2\text{O}}} = m, \quad (8)$$

where m , the ligation number, is the slope of a trend describing the experimental data by the orthogonal coordinates, $\log f_{\text{AuCl}_m(\text{H}_2\text{O})_n}$ and $\log f_{\text{HCl}}$. In Figure 12A, the data for gold are shown in these coordinates at 300°C, and, as can be seen from this diagram, the slope is ~ 1 , indicating that Au and Cl are present in the gas species in a 1/1 ratio (as fugacity coefficients for HCl and the Au species are not known, it was assumed that $P_{\text{gas}} = f_{\text{gas}}$). The same slope was obtained at 340° and 360°C. As discussed for silver and copper, this 1/1 ratio does not necessarily indicate the stoichiometry of the inner sphere complex, but as there are no comparable data for the H_2O -free system $\text{Au(I)}\text{-Cl}$, it was tentatively assumed that the species in the experiments had the stoichiometry AuCl (Archibald et al., 2001).

The hydration number of the different metal species in the vapor was calculated by differentiating the logarithm of the expression for the equilibrium constant of the speciation reaction with respect to $\log f_{\text{H}_2\text{O}}$, holding f_{O_2} and f_{HCl} constant. Using the example of the gold speciation reaction (eq. 5) to illustrate this process, it can be seen that differentiation of equation (6) with respect to $\log f_{\text{H}_2\text{O}}$ yields:

$$\left(\frac{\partial \log K_f}{\partial \log f_{\text{H}_2\text{O}}} \right)_{T, f_{\text{HCl}}, f_{\text{O}_2}} = 0 = \left(\frac{\partial \log f_{\text{AuCl}_m(\text{H}_2\text{O})_n}}{\partial \log f_{\text{H}_2\text{O}}} \right)_{T, f_{\text{HCl}}, f_{\text{O}_2}} + \frac{m}{2} \cdot \left(\frac{\partial \log f_{\text{H}_2}}{\partial \log f_{\text{H}_2\text{O}}} \right)_{T, f_{\text{HCl}}, f_{\text{O}_2}} - \left(\frac{\partial \log f_{\text{Au}}}{\partial \log f_{\text{H}_2\text{O}}} \right)_{T, f_{\text{HCl}}, f_{\text{O}_2}} - n \left(\frac{\partial \log f_{\text{H}_2\text{O}}}{\partial \log f_{\text{H}_2\text{O}}} \right)_{T, f_{\text{HCl}}, f_{\text{O}_2}} \quad (9)$$

Thus

$$\left(\frac{\partial \log f_{\text{AuCl}_m(\text{H}_2\text{O})_n}}{\partial \log f_{\text{H}_2\text{O}}} \right)_{T, f_{\text{O}_2}, f_{\text{HCl}}} = n - \frac{m}{2} - \left(\frac{\partial \log f_{\text{Au}}}{\partial \log f_{\text{H}_2\text{O}}} \right)_{T, f_{\text{O}_2}, f_{\text{HCl}}} \quad (10)$$

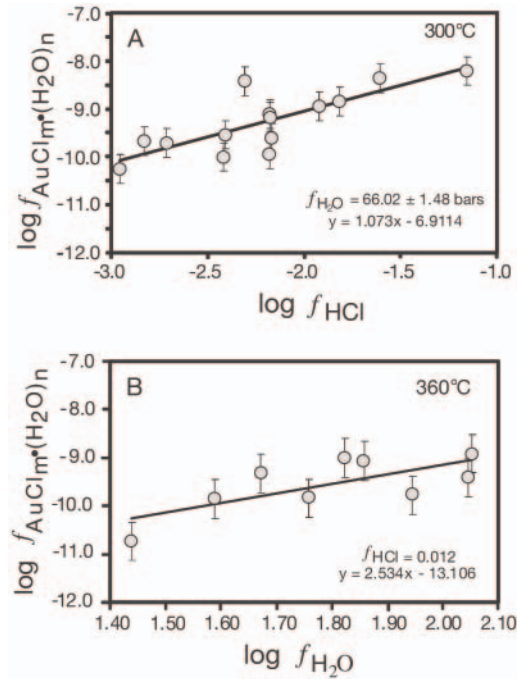


FIG. 12. A. The log fugacity of the gas species $\text{AuCl}_m(\text{H}_2\text{O})_n$ as a function of $\log f_{\text{HCl}}$ at constant $f_{\text{H}_2\text{O}}$ (modified after Archibald et al., 2001). The subscripts m and n refer to the ligation number of the inner sphere complex and the hydration number, respectively. The slope of ~ 1 of the linear regression through the experimental data indicates that the ligation number (m) is 1 and therefore that the inner sphere complex has the stoichiometry, AuCl . B. The log fugacity of the gas species $\text{AuCl}_m(\text{H}_2\text{O})_n$ as a function of $\log f_{\text{H}_2\text{O}}$ at constant f_{HCl} . The slope of the linear regression through the experimental data (2.53) corresponds to the right-hand side of equation (10). As m is 1 and the Gibbs Poynting correction (from a heterogeneous gas-solid to a gas-only system) for these data is ~ 0.11 , the corresponding statistical hydration number (n) is 3.14. See text for further details.

(the derivative of the log fugacity of H_2 with respect to the log fugacity of H_2O equals unity at constant fugacity of O_2). As the system investigated was not homogeneous (i.e., it contained both solid and vapor), a Gibbs-Poynting correction was applied to make it effectively homogeneous for the purpose of thermodynamic description. This involved correcting the change in the partial pressure of Au^{gas} over the crystalline phase from that for a total pressure of $P_1 = 1$ bar (standard state) to that for P_2 , the pressure of the run:

$$\ln \frac{f_2^\circ}{f_1^\circ} = \frac{V^\circ \cdot (P_2 - P_1)}{R \cdot T}, \quad (11)$$

where V° is the molar volume and f_1° and f_2° are the fugacities of this component in states 1 and 2.

Substitution of equation (11) into equation (10) results in the following expression:

$$\left(\frac{\partial \log f_{\text{AuCl}_m(\text{H}_2\text{O})_n}}{\partial \log f_{\text{H}_2\text{O}}} \right)_{T, f_{\text{O}_2}, f_{\text{HCl}}} = n - \frac{m}{2} - \left(\frac{V^\circ \cdot (P_2 - P_1)}{R \cdot T} \right). \quad (12)$$

The slope of a trend describing the experimental data by the orthogonal coordinates, $\log f_{\text{AuCl}_m(\text{H}_2\text{O})_n}$ and $\log f_{\text{HCl}}$ (Fig. 12B)

yields the right-hand side of equation (12), and as the values of all other parameters on this side of the equation except n , the hydration number, are known, the equation can be solved for n .

This analysis yielded hydration numbers, which varied according to the system investigated and in some cases varied significantly with temperature in the same system. Thus, whereas the hydration number was three for the silver gas species ($\text{AgCl} \cdot 3\text{H}_2\text{O}^{\text{gas}}$) over the range of temperatures investigated, for gold it decreased from five at 300°C to three at 360°C (Table 5). A similar finding was obtained for copper, consistent with the observation that these two metals undergo retrograde solubility (Archibald et al., 2001, 2002). Overall, these hydration numbers are similar to those found in aqueous liquids. In the case of silver, they predict that the metal is coordinated by three molecules of water and one of chlorine (i.e., that it is in tetrahedral coordination). Significantly, Monte Carlo and molecular dynamic simulations of the hydration of Ag^+ in the vapor phase predict the same coordination (Abraham and Matteoli, 1983; Shevkunov, 1996; Martinez et al., 1997). Moreover, the coordination of the first hydration shell around Ag^+ in aqueous solutions has been shown to be tetrahedral using electron-spin echo modulation (Kevan et al., 1977), ultraviolet spectroscopy (Texter et al., 1983), and X-ray absorption spectroscopic studies (EXAFS: Seward et al., 1996).

TABLE 5. Hydration Numbers for Metallic Species in Water Vapor and Equilibrium Constants for Reactions Describing the Formation of These Species

T (°C)	n	log K
$\text{AgCl}^{\text{cryst}} + n\text{H}_2\text{O} = \text{AgCl}(\text{H}_2\text{O})_n^1$		
360	3	-12.53
350	3	-12.537
340	3	-12.507
330	3	-12.707
310	3	-12.668
300	3	-12.975
$\text{Au}^{\text{metal}} + \text{HCl} + n\text{H}_2\text{O} = \text{AuCl}(\text{H}_2\text{O})_n + 0.5 \text{H}_2^2$		
300	5	-17.28
340	4	-18.73
360	3	-18.74
$3 \text{CuCl}^{\text{cryst}} + n\text{H}_2\text{O} = \text{Cu}_3\text{Cl}_3(\text{H}_2\text{O})_n^3$		
280	7.6	-21.46
300	6	-19.03
320	6.1	-19.45
$\text{SnO}_2^{\text{cryst}} + 2\text{HCl} + n\text{H}_2\text{O} = \text{SnOCl}_2(\text{H}_2\text{O})_{n+1}^4$		
300	1.9	-8.48
320	1.7	-7.29
350	1.5	-7.27

¹ Migdisov et al. (1999)

² Archibald et al. (2001)

³ Archibald et al. (2002)

⁴ Migdisov and Williams-Jones (2005)

Thermodynamic data

In order to be able to apply the results of the experiments to natural systems, the solubility data were used to calculate equilibrium constants for the different speciation reactions postulated. Unfortunately, except for the Ag species, there was no justification in extracting thermodynamic data, such as the Gibbs free energy, entropy and heat capacity, as the hydration number, and thus the nature of the metallic species in the vapor changed with temperature. To illustrate how the formation constants for the metallic species were calculated, we continue with the example of gold. As discussed above, the speciation reaction for gold is given by equation (5) and the expression for the corresponding equilibrium constant by equation (6). However, as gold in its standard state is a solid, equation (6) must be modified by replacing Au^{gas} with Au^{solid} as follows:

$$\text{Au}^{\text{solid}} + m \cdot \text{HCl}^{\text{gas}} + n \cdot \text{H}_2\text{O}^{\text{gas}} = \text{AuCl}_m \cdot (\text{H}_2\text{O})_n^{\text{gas}} + \frac{m}{2} \cdot \text{H}_2^{\text{gas}}, \quad (13)$$

and

$$\log K_f = \log f_{\text{AuCl}_m \cdot (\text{H}_2\text{O})_n} + \frac{m}{2} \cdot \log f_{\text{H}_2} - n \cdot \log f_{\text{H}_2\text{O}} - m \cdot \log f_{\text{HCl}}. \quad (14)$$

The value of $\log K_f$ can thus be calculated knowing $f_{\text{AuCl}_m \cdot (\text{H}_2\text{O})_n}$, f_{H_2} , f_{HCl} , and $f_{\text{H}_2\text{O}}$, and, as the last three parameters were evaluated as part of the experimental methodology (see above) only $f_{\text{AuCl}_m \cdot (\text{H}_2\text{O})_n}$ remains to be evaluated. This was done from the concentration of gold in the quenched condensate, assuming that the mole fraction of gold is given by the equation:

$$X_{\text{AuCl}_m \cdot (\text{H}_2\text{O})_n} \equiv \left(\frac{M_{\text{AuCl}_m \cdot (\text{H}_2\text{O})_n}}{M_{\text{H}_2\text{O}}} \right), \quad (15)$$

where M is the number of moles of the corresponding compound (the effect of M_{HCl} on the total mass of fluid in the autoclave was assumed to be negligible). Assuming that the species in the vapor phase form an ideal gas mixture, it therefore follows that:

$$X_{\text{AuCl}_m \cdot (\text{H}_2\text{O})_n} \equiv \left(\frac{f_{\text{AuCl}_m \cdot (\text{H}_2\text{O})_n}}{f_{\text{H}_2\text{O}}} \right), \quad (16)$$

or

$$f_{\text{AuCl}_m \cdot (\text{H}_2\text{O})_n} = X_{\text{AuCl}_m \cdot (\text{H}_2\text{O})_n} \cdot f_{\text{H}_2\text{O}}. \quad (17)$$

Values of $\log K_f$ calculated in this manner for the different metallic species investigated in the experiments described above are listed in Table 5.

Implications for natural systems

The most important conclusions that can be drawn from the experiments summarized above are that (1) in all cases

there is a positive logarithmic correlation of metal solubility with partial pressure of water vapor, (2) the metallic species in the vapor phase is hydrated, and (3) the partial pressure or solubility of this species is many orders of magnitude greater than the values predicted for ideal systems based on the dry volatility of metallic solids. It thus follows that, because of its power of solvation (hydration), water vapor is a much more effective agent of metal transport than previously suspected.

It is important to note that calculations employing the equilibrium constants listed in Table 5 are valid only for the conditions of the experiments, and that the latter were designed for systems with properties approaching those of pure water (i.e., in which vapor is only stable at pressures below ~220 bars). However, many natural ore-forming hydrothermal systems, notably those associated with subduction-related magmatism, are characterized by high salinity, and in such systems, two-phase behavior extends to much higher pressure than for pure water (Fig. 2). Therefore, as the solubility of metals in water vapor increases strongly with increasing water fugacity, the already significant solubilities of metals in pure water vapor will increase to even higher values in the more dense vapor phase existing at higher pressures in high-salinity saline fluid systems. In addition to the solubility-enhancing effect of increasing hydration with higher water pressure, the presence of chloride and sulfur species as complexing ligands will further enhance the metal-transporting capacity of the more dense vapor in natural systems. The recent experiments, although of still quite limited applicability, are thus in accord with the observation of orders of magnitude greater concentration of ore metals in natural vapor inclusions compared with low-pressure volcanic vapors.

Magmatic Vapor in Porphyry-Epithermal Systems: Source, Ascent, and Mineral Deposition

Recent fluid inclusion studies of ore-forming magmatic-hydrothermal systems, including those generating porphyry copper and epithermal gold deposits, indicate a far more

important role for magmatic vapor as a metal-transporting ore fluid than is generally acknowledged. Returning to some of the pioneering ideas of Henley and McNabb (1978) and Eastoe (1982), we propose an interpretation of fluid processes in which the vapor phase is the main agent of mass transfer, linking hydrous magmas to porphyry-type and epithermal ore deposits. A key consideration in interpreting the range of compositions and pressure-temperature-density conditions experienced by magmatic-hydrothermal fluids is that low- to moderate-salinity fluids have a continuous stability range, extending from a low-density vapor at high temperature and low pressure to an intermediate-density fluid at elevated pressure and intermediate temperature to a dense aqueous liquid at lower temperature and any pressure above the boiling surface (Fig. 2). Such continuity in fluid stability implies that a single-phase magmatic vapor ($\rho < \rho_{\text{critical}}$) can cool and contract to an aqueous liquid ($\rho > \rho_{\text{critical}}$) at lower temperature without breaching the two-phase surface and changing its composition. Thus, even liquid-like epithermal ore fluids of low salinity may be entirely magmatic in origin and may have acquired their metal load from a precursor vapor-like fluid that exsolved directly from a silicate melt (Hedenquist et al., 1998) or separated from a hypersaline aqueous liquid (Fig. 13).

Figures 13 and 14 schematically depict three fluid regimes in which vapor-driven mass transfer plays a dominant role: (1) in fumarole-related alteration and volatile metal deposition, (2) in porphyry Cu-(-Mo-Au) mineralization, and (3) in the transport of gold and copper into epithermal ore-forming environments. The key factor distinguishing these fluid regimes is the depth at which fluids exsolve from hydrous magma and the resulting pressure-temperature paths followed by them en route to the surface. The three fluid regimes may develop separately at different depths above the magma chamber and produce three correspondingly different ore deposits. Alternatively, and particularly when a vertically extensive magma body gradually cools and isotherms retract to great depth above the fluid-exsolving front of the

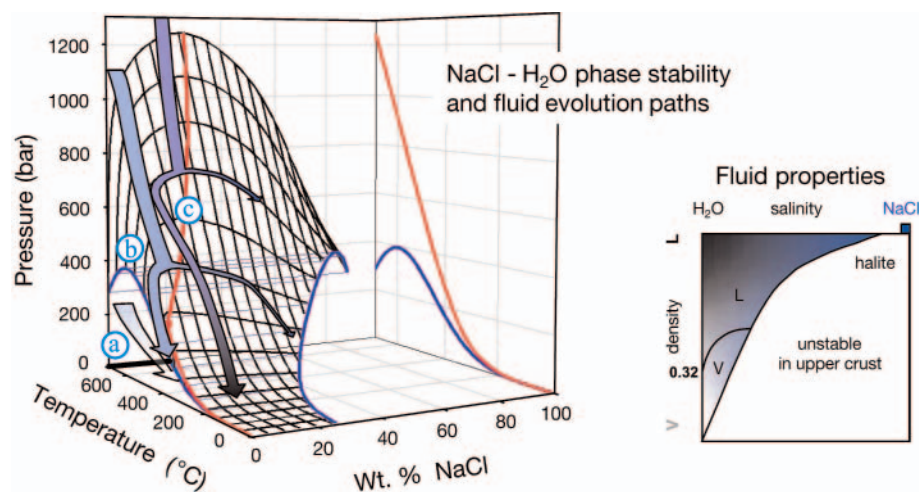


FIG. 13. NaCl-H₂O phase diagram represented in Figure 2, showing three possible paths of fluid evolution illustrated by arrows, two of which bifurcate where a single-phase fluid intersects the two-phase surface and separates into a lower salinity vapor and a higher salinity liquid (brine). Fluid characteristics are indicated by varying color shade (salinity) and darkness (density) along the arrows, according to the approximate scale shown in the inset (right); L and V refer to liquid and vapor.

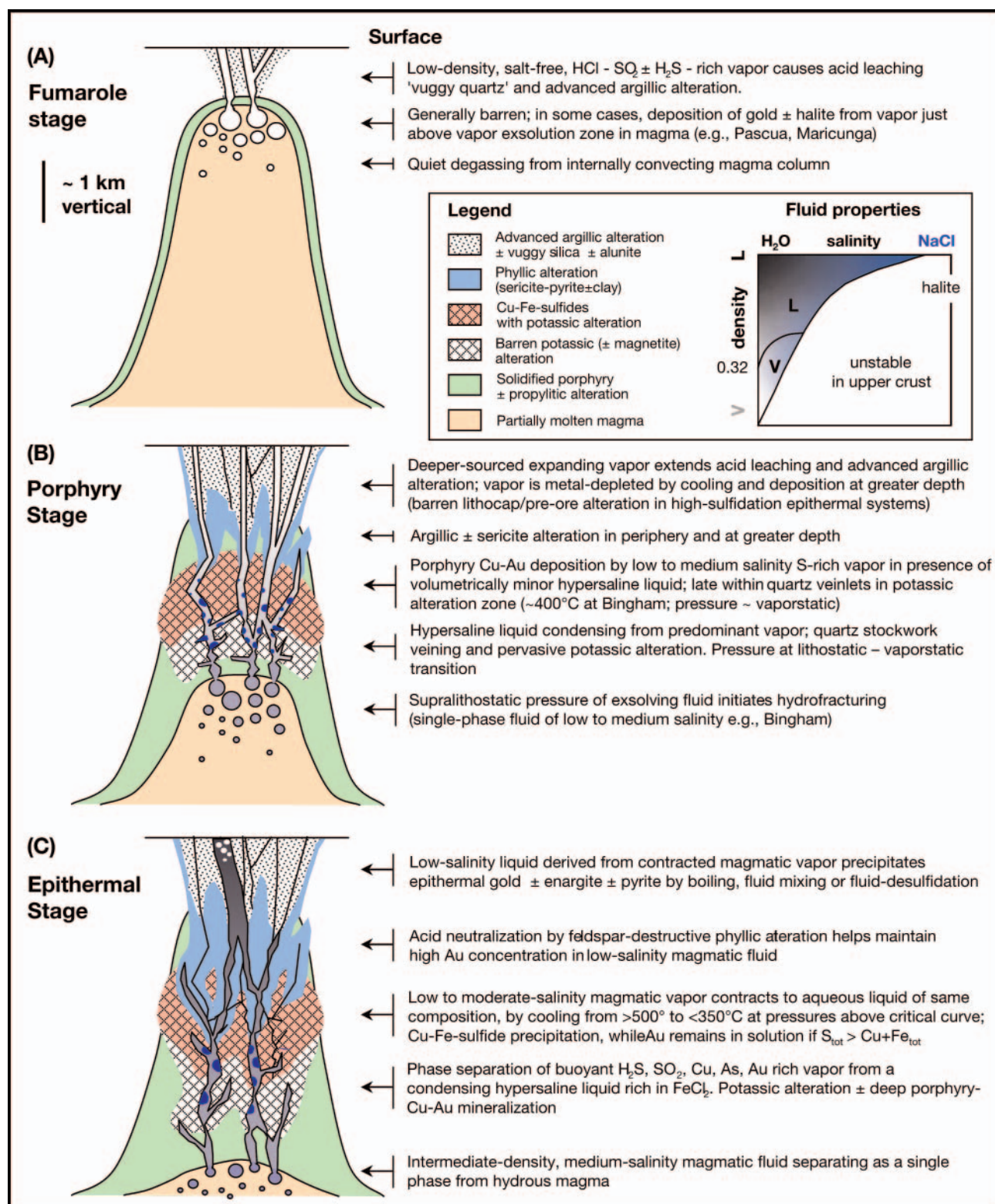


FIG. 14. Schematic cross sections showing three fluid evolution regimes, which may occur separately above magma chambers emplaced at different depths or develop sequentially during evolution of a single, vertically extensive porphyry to epithermal system, as the fluid-producing magmatic interface retracts to greater depth during cooling. The fluid evolution paths in the three sections correspond to those shown in Figure 13, as do the darkness and/or shade of color used to depict density, salinity, and phase state of fluids in schematically indicated fracture channelways. Fluid processes, rock alteration, and mineral precipitation are explained by text at the corresponding level to the right of each section. Successive overprinting of magmatic vapor processes may proceed from an early fumarole stage (A) through a porphyry stage (B) to a final epithermal stage (C) as a result of overall cooling and retraction of the fluid-generating magma front toward a subjacent magma chamber.

crystallizing magma chamber, these three regimes may spatially overlie and temporally overprint each other, leading to a characteristic overprinting of ore and alteration styles. In the following sections, we discuss the three fluid regimes, using specific geologic examples exposed at different erosional levels.

Fumarole-related ore deposits

Magmatic vapors emanating from active volcanoes or shallow subvolcanic intrusions at near-atmospheric pressure are salt poor but usually rich in SO_2 , H_2S , and HCl , leaving behind some hypersaline liquid or solid salt, as shown by arrow "a" in Figure 13 and in the schematic part A of Figure 14. The vapor typically condenses on cooling (Fig. 13; tip of arrow "a") to form an extremely acid liquid rich in HCl and H_2SO_4 . Such fluids are responsible for the halos of advanced argillic alteration (kaolinite, pyrophyllite, alunite) and intense rock leaching (e.g., residual vuggy quartz) observed around fumaroles (Delmelle and Bernard, 1994) and as hosts to high-sulfidation epithermal $\text{Au} \pm \text{Cu} \pm \text{As}$ deposits (Ransome, 1907; Brimhall and Ghiorso, 1983; Stoffregen, 1987; Landis and Rye, 2005). The magmatic vapors causing this alteration may also transport the ore metals and form economic deposits by precipitation directly from the vapor phase or after condensation into meteoric water.

Mercury deposits: Some clearcut examples of metal transport by the vapor phase are provided by mercury deposits (Varekamp and Busek, 1984), which generally form in steam-heated geothermal environments hosted by highly reducing rocks (organic-rich sediments or serpentinites). The Ngawha geothermal field in New Zealand is a vapor-dominated system in which mercury precipitates as cinnabar and liquid metal in swamp sediments rich in organic material and locally condenses as liquid metal on open metal surfaces, such as roof guttering (Davey and van Moort, 1987; Barnes and Seward, 1997). Mercury transport by a low-density vapor phase is envisaged for the formation of the Culver-Baer deposit (Peabody and Einaudi, 1992) and other deposits in California (White et al., 1971). The metal sources of the world's largest mercury deposits, Almadén (Spain: Saupé and Arnold, 1992) and Idrija (Slovenia: Palinkas et al., 2004), are inferred to be in black shales that also host the deposits. Fluid inclusions in cinnabar and associated gangue minerals indicate that Hg was mobilized by a variably saline aqueous liquid rather than a low-density vapor. However, both deposits show evidence of coeval mantle-derived magmatism (rift basalts and alkali basaltic diatremes), so that an input of Hg-rich magmatic vapor at depth cannot be excluded.

Mexican-type tin deposits: Another example of metal transport by vapor is provided by rhyolite-hosted tin deposits, containing microcrystalline cassiterite known as "wood tin," which initially were thought to have formed from vapors exsolved directly from F-rich rhyolite flows at near-atmospheric pressure (Duffield et al., 1990). Subsequent melt inclusion studies led Webster et al. (1996) to conclude that the Sn-F-rhyolite magmas were already volatile saturated prior to extrusion, which is consistent with the conclusion from experimental studies (above) that a somewhat denser magmatic vapor phase is more likely to transport economic metal concentrations than a fumarolic vapor at atmospheric pressure.

Advanced argillic alteration in high-sulfidation epithermal deposits: In most high-sulfidation epithermal systems, advanced argillic alteration predates metal introduction (Cu-As followed by Au-Ag-As) by later aqueous fluids of low to intermediate salinity and liquid-like density (Stoffregen, 1987; Berger and Henley, 1989; Arribas, 1995; Heinrich, 2005). However, in some high-sulfidation deposits, including the Pascua deposit in Chile, mineralization appears to have been contemporaneous with acid leaching and alteration (Chouinard et al., 2005a), indicating that gold and associated copper may have been deposited directly from a low-density magmatic vapor or its condensate. Even without considering possibly more volatile Au-S species, the experimentally determined concentration of gold in a low-density vapor phase at the conditions typical of epithermal environments (e.g., at 300°C , 80 bars $\text{P}_{\text{H}_2\text{O}}$, 0.3 m Cl , $\text{pH} \sim 1$, and $\log f_{\text{O}_2} \sim -28$) would be ~ 1 ppb Au , an amount that theoretically is sufficient to produce an economic gold deposit within the typical lifespan of hydrothermal systems (Archibald et al., 2001; see also Hedenquist et al., 1993). Interestingly, over 50 percent of the gold at Pascua is incorporated in the structure of pyrite and enargite, which Chouinard et al. (2005b) have attributed to gold adsorption onto sulfide surfaces, a potentially effective mechanism for scavenging gold from a relatively Au poor vapor that may have been undersaturated with respect to native gold (see also Palenik et al., 2004). Metal transport by a low-density vapor may also have formed the banded quartz veinlets characterizing the porphyry gold deposits of the Maricunga belt of northern Chile. These veinlets are unusual in containing dark botryoidal, inclusion-rich quartz and a fluid inclusion population comprising over 99 percent vapor inclusions without recognizable liquid. Muntean and Einaudi (2000) interpreted these features to reflect the unusually shallow level of intrusion (<1 km), which led to exsolution of a brine-vapor mixture that flashed in response to abrupt decompression from a <250 -bars lithostatic pressure to a hydrostatic pressure of <100 bars. They concluded that the gold was transported in the brine and that the flashing led to its supersaturation and deposition from this phase. However, it is equally reasonable to infer that the exsolved fluid was dominantly vapor, and that this phase transported the gold, which subsequently deposited in response to a sharp density reduction, accompanying expansion of the vapor into open veins. This latter interpretation is consistent with experimental evidence that gold solubility decreases sharply with decreasing $\text{P}_{\text{H}_2\text{O}}$ (Fig. 12B).

Although low-density fumarolic vapors may deposit economic amounts of gold and copper, metal concentrations in such vapors are predicted to be generally too low for ore formation. This is despite the fact that appreciable quantities of Cu and probably other ore metals are transferred to the vapor phase by low-pressure devolatilization of hydrous lavas, as shown by Cu -enriched vesicles (Lowenstern et al., 1991) and by the low bulk Cu content of lavas compared to that of melt inclusions contained in phenocrysts (Halter et al., 2005). Instead of transporting these metals to efficient ore traps, the low-density vapor phase will, in most cases, simply disperse them into the atmosphere and near-surface waters. Much greater transport efficiency is predicted for more dense vapor at higher pressure and temperature, as discussed below, and

such a fluid is also more likely to follow a cooling path leading to trapping of the metals in high-grade orebodies.

Formation of porphyry Cu-Au-Mo ore by expanding vapor

The salinity, density, and phase state of magmatic fluids involved in porphyry copper (\pm Au \pm Mo) mineralization are variable, as indicated by fluid inclusion assemblages in and below the deposits. Exsolution of magmatic volatiles from a crystallizing hydrous magma can occur in the single-phase fluid stability region at high pressure ($>1,000$ bars) or brine and vapor may separate simultaneously from the magma if its solidus intersects the two-phase surface of the salt-water fluid system. Direct two-phase fluid exsolution from silicate melt may occur if the pressure is relatively low ($<1,000$ bars) or if the Cl/OH ratio in the melt is relatively high (Burnham, 1979; Bodnar et al., 1985; Cline and Bodnar, 1991; Cline, 1995; Webster et al., 1999; Ulrich et al., 2001; Audétat and Pettke, 2003).

In the majority of porphyry copper deposits, potassic alteration and Cu-Fe sulfide deposition occur in the stability field of two coexisting fluids, as recorded by intimately associated brine and vapor inclusions. Boiling trails typically indicate pressures between 300 and 1,200 bars, which correspond to a lithostatic load of 1 to 4 km of overburden (e.g., Roedder, 1984; Alumbraer et al., 2001; Bingham Canyon: Redmond et al., 2004). Some porphyry deposits, including Butte, formed at pressures in excess of 2,000 bars from a single-phase magmatic fluid of relatively low salinity (~ 4 wt % NaCl equiv) and liquid-like to near-critical density ($0.7\text{--}0.4$ g cm $^{-3}$; Rusk et al., 2004). Others, like the Far South East porphyry Cu-Au deposit in the Philippines, which was emplaced at the cool and shallow end of the porphyry spectrum, at a depth of 1 to 2 km based on geologic evidence, also formed from a relatively low salinity magmatic liquid. The Cu-Au deposition occurred during sericitization, which overprinted early weak potassic alteration associated with a hotter two-phase fluid (brine + vapor; Hedenquist et al., 1998).

Although great emphasis has been placed on the study of the spectacular and relatively easy to measure brine inclusions present in many porphyry deposits, fluids of low to moderate salinity (2–10 wt % NaCl equiv) but highly variable density are the most widespread inclusion type. Unlike brine inclusions, low-salinity fluid inclusions are common in all porphyry copper deposits and commonly also represent the most abundant inclusion type during the ore-forming stage (e.g., Bingham Canyon: Fig. 7C; Bell: Wilson et al., 1980). Microanalyses of low-salinity fluid inclusions from porphyry Cu and skarn deposits (App.) show elevated to very high Cu/Na ratios (up to 1 in many cases), commonly exceeding the Cu/Na ratio expected from partitioning experiments involving intermediate to felsic silicate melts and chloride fluids in the single-phase (Candela and Holland, 1986; Candela, 1989a; Candela and Piccoli, 1995) or in the two-phase fluid stability field (Williams et al., 1995). Sulfur is difficult to analyze in fluid inclusions, and results of experiments involving sulfur are still not conclusive (Nagaseki and Hayashi, 2004; Simon et al., 2005c), but it seems highly likely that the variably high Cu and Au contents in porphyry-related low-salinity fluids is due to the formation of sulfur-bearing metallic gas species.

The distribution of fluid inclusions in the deeply explored Bingham Canyon porphyry Cu-Au system (Fig. 7) indicates

that low-salinity vapor was the dominant agent of metal transport for that deposit. Fluids trapped as a single-phase fluid ~ 1 km below the Bingham orebody have near-critical density and salinities that are similar to those of vapor inclusions in the overlying orebody (both <11 wt % NaCl equiv), and both fluids are at least four times less saline than the brine inclusions coexisting with vapor inclusions within the orebody (Redmond et al., 2004; Landtwing et al., 2005). If the vapor and brine are indeed derived from the deep near-critical fluid by phase separation, as a result of decompression near the lithostatic to hydrostatic transition (Redmond et al., 2004), then mass balance imposed by the salinity relationships indicates that only a small proportion of brine ($<25\%$ by mass) can have condensed from the ascending fluid, which was dominated by vapor ($>75\%$ by mass). Indeed, the highest Cu/Na ratios in the intermediate-density fluid are similar to those in the vapor (prior to Cu-Fe sulfide deposition), and both low-salinity fluids have higher Cu/Na ratios than the brine.

These data suggest that Bingham Canyon formed according to the process shown schematically in part B of Figure 14. A single-phase fluid ascending from a hidden magma chamber beneath the Quartz Monzonite Porphyry (Fig. 7) started to condense a relatively small fraction of brine after intersecting the two-phase surface on the vapor side of the critical curve (Fig. 13; branching point of arrow "b") but without significantly changing its composition. The expanding vapor ascended further in the presence of minor brine, reaching Cu-Fe sulfide saturation as the coexisting fluids cooled below 425°C near the sharply defined base of the orebody (Fig. 7). The vapor phase was the dominant fluid in terms of the total mass of H $_2$ O, of Cu, and probably even of Cl. This explains why bornite and chalcopyrite precipitation, which occurred between 425° and 350°C , was accompanied by dissolution of quartz (shown by cathodoluminescence imaging; Redmond et al., 2004; Landtwing et al., 2005) because, in this temperature interval, the solubility of silica is retrograde in low-salinity fluids (Fournier, 1999). In high-salinity fluids, silica solubility is prograde and, consequently, dissolution of quartz would not have occurred if the brine were the dominant mineralizing fluid. Salt mass balance and quartz dissolution are, therefore, two independent reasons to conclude that the vapor was the main ore fluid at Bingham, whereas the coexisting brine (although providing a better quantifiable fluid inclusion record during Cu-Fe sulfide precipitation) never carried more than a small fraction of the total metal that is now contained in the giant Bingham Canyon orebody. The spent ore fluid may have expanded to a low-density vapor contributing to advanced argillic alteration above the present mine level, as sketched in part B of Figure 14 for a system in which fluid pressure above the ore zone approaches vapor-static conditions. Other fluid aliquots may have contracted to aqueous liquid along hydrologically more constrained pathways, due to vein sealing by reprecipitation of late quartz (Fournier 1999; Redmond et al., 2004; Landtwing et al., 2005) and may thus have contributed to the formation of sediment-hosted epithermal gold deposits in the vicinity (Sillitoe and Bonham 1990; see discussion of part C of Fig. 14, below).

Cotransportation of S, Cu, and Au by magmatic vapor implies that the supply of sulfur by the igneous fluid source may be the limiting factor in the generation of economic porphyry copper deposits (cf. Gustafson and Hunt, 1975). A sulfide

deficit in the magma could explain the exceptionally low Cu concentrations in vapor inclusions from the barren Rito del Medio pluton, which otherwise has normal Cu contents in the coexisting brine (App.; Audétat and Pettke, 2003). By contrast, exceptionally high sulfur availability with only modestly elevated copper contents characterize the magmas of the Farallón Negro Volcanic Complex that formed the Bajo de la Alumbrera porphyry Cu-Au deposit, as indicated by Cu, Au, and S mass-balance constraints from the composition of silicate and sulfide melt inclusions (Halter et al., 2005).

Contracting vapor to liquid: The link to epithermal gold

Paragenetic vein relationships and fluid inclusion data indicate that economic gold (Cu, As \pm Ag) deposition even in high-sulfidation ore deposits is generally not effected by the acid vapor but by an aqueous liquid of somewhat lower acidity and low to intermediate salinity that enters the deposits through veins that postdate acid leaching of the wall rocks (e.g., Stoffregen, 1987; Arribas, 1995; Hedenquist et al., 1998; Heinrich, 2005). This fluid is similar to the low- or moderate-salinity aqueous fluid trapped in quartz-sericite-pyrite \pm chalcopyrite veins underlying some high-sulfidation gold deposits (e.g., Rodalquilar; Arribas et al., 1995) and cutting through the upper parts of many porphyry copper deposits (Gustafson and Hunt, 1975; Hedenquist et al., 1998).

The low-salinity, aqueous liquids that form most epithermal deposits are commonly interpreted to be meteoric in origin, with small magmatic contributions for high-sulfidation systems (Taylor, 1974; Berger and Henley, 1989; Hedenquist et al., 1994). However, early studies of gold deposits of low- to intermediate-sulfidation state showed evidence for a significant involvement of magmatic fluid (Silberman and O'Neil, 1974), and more recent studies of the Transylvanian Au-Ag-Te deposits of Romania support this interpretation (Alderton and Fallick, 2000; K. Kouzmanov and T. Vennemann, unpub. data). In addition, stable isotope data indicate that the fluid responsible for early advanced argillic alteration associated with high-sulfidation deposits is dominantly magmatic (Rye et al., 1992; Rye, 1993; Vennemann et al., 1993; Hedenquist et al., 1998). Thus, there appears to be a growing recognition of the importance of magmatic fluids in the formation of a wide variety of epithermal deposits.

Low-salinity magmatic liquid can originate by cooling from the single-phase stability region without ever intersecting the two-phase surface (Hedenquist et al., 1998; Muntean and Einaudi, 2001). Alternatively, this fluid can form by separation of vapor from brine at near-magmatic temperatures and pressures, and subsequent cooling and contraction of the vapor to an aqueous liquid (Heinrich et al., 2004; Heinrich, 2005). This process is indicated by arrow "c" in Figure 13 and depicted schematically in part C of Figure 14. Vapor can be cooled in the single-phase stability field along any pressure-temperature path that passes above the critical curve to lower temperature and thereby will contract from a vapor-like state to an aqueous liquid without crossing any phase boundary. The resulting magmatic-hydrothermal liquid, although originally derived from a vapor of the same composition, may eventually boil or mix in any proportion with aqueous liquids of meteoric origin (Fig. 14C).

Fluid inclusion analyses discussed above indicate that a deep magmatic source can generate weakly saline vapor with

Cu, As, and Au concentrations that are many orders of magnitude higher than those in geothermal liquids or in low-density vapor at epithermal conditions. A key question is how an intervening step of brine-vapor separation at high temperature and pressure (~ 450 – 600°C , 400–1,000 bars) affects the chemical composition of the vapor and its ability to transport ore metals, notably gold, to the much cooler epithermal ore environment. Below 400°C , experimental data for the stability of metal complexes in aqueous fluids (Gammons and Williams-Jones, 1995; Benning and Seward, 1996; Xiao et al., 1998; Stefánsson and Seward, 2004) permit quantitative calculation of gold and copper solubility in cooling magmatic-hydrothermal fluids (Heinrich, 2005). If the total concentration of FeCl_2 in a high-temperature fluid exceeds that of H_2S , the precipitation of pyrite and Cu-Fe sulfide minerals will lead to rapid exhaustion of reduced sulfur during cooling, which will cause deposition of Au with Cu-Fe sulfides at high temperature and severely limit the ability of a low-salinity fluid to transport gold into the epithermal environment. If, on the other hand, partitioning of an FeCl_2 into a high-salinity brine increases the molality ratio of $\text{H}_2\text{S}/\text{Fe}$ in the high-temperature vapor, then FeS_2 precipitation during subsequent cooling and contraction of the vapor may lead to an Fe-depleted but still sulfide-rich aqueous liquid at lower temperatures. Such a low-salinity magmatic-hydrothermal liquid may carry very high concentrations of gold even at epithermal temperatures well below 300°C (Gammons and Williams-Jones, 1997), at parts per million levels as analyzed in porphyry-hosted vapor inclusions (Ulrich et al., 1999) rather than at parts per billion levels as observed in volcanic vapors or in rock-buffered geothermal waters of meteoric origin.

Thermodynamic modeling detailed in Heinrich (2005) shows that wall-rock reaction also critically influences the ability of a vapor-derived fluid to transport high concentrations of gold to the epithermal environment. A high degree of rock interaction with Fe-bearing wall rocks (approximating a rock-dominated chemical evolution) will deplete the fluid in H_2S and lead to precipitation of gold at high temperature (e.g., together with pyrite and chalcopyrite in late porphyry veins). Complete isolation of the fluid from the wall rocks, by channeling into fractures, also leads to precipitation of gold at high temperature (e.g., along quartz veins), because internal equilibria drive the fluid to very low pH (fluid-buffered cooling). However, at intermediate degrees of wall-rock interaction, which can occur in the pH region of quartz + sericite \pm pyrophyllite stability, the fluid can transport at least 1 ppm of gold across a large interval of cooling from $>400^\circ\text{C}$ to epithermal temperatures as low as 150°C . Such a vapor-derived, partially rock-reacted, aqueous liquid is thus predicted to be the most effective agent for producing high-grade epithermal gold deposits.

In our opinion, the differences among epithermal precious metal deposit types distinguished on the basis of sulfide mineral paragenesis (e.g., sulfidation state) and alteration style (pH) are not due primarily to a different source of the main gold-introducing fluid, which we propose to be a vapor-derived low-salinity magmatic liquid. Instead, we suggest that the differences in epithermal ore and alteration mineralogy result primarily from differences in the pressure-temperature evolution of brine and vapor and from relatively subtle

differences in the degree of interaction of the low-salinity ore fluids with wall rocks prior to their arrival at the site of ore deposition. These differences in fluid evolution are further accentuated by differences in the chemical processes operating at the deposition site, such as highly acidic preore alteration in high-sulfidation systems, or boiling, reduction, or mixing of gold-rich magmatic fluid with predominantly meteoric water to form high-grade zones in epithermal veins of low- to intermediate-sulfidation state.

Conclusions and Outlook

The combination of experimental and geologic evidence summarized in this paper shows that vapor can play a major role as a medium for ore-metal transport in the formation of magmatic-hydrothermal ore deposits. Two fundamental conclusions regarding the metal-transporting capacity of vapor emerge from studies of active volcanoes, microanalyses of natural fluid inclusions, laboratory experiments, and thermodynamic analysis.

First, the metal-transporting capacity of aqueous vapor increases dramatically with increasing water fugacity, due to the hydration of inner sphere metal-ligand complexes to form species of the type $\text{MeL}_{m,n}\text{H}_2\text{O}$. As a result, metal solubility in water-rich vapor depends not only on the available ligands (e.g., Cl, S, as in aqueous liquids) but also on the density of the water-dominated vapor, which increases with increasing pressure. Hydration explains measured metal concentrations in low-pressure volcanic vapors, that are orders of magnitude higher than those calculated from the dry volatility of metal salts but generally too low to be effective ore fluids. As expected from the hydration experiments, base and precious metal concentrations are much higher in dense vapor inclusions, in which percent levels of Cu and parts per million levels of Au have been analyzed.

Second, vapor transport may contribute to the selective enrichment of certain metals (e.g., Cu and Au), if these metals are partitioned preferentially into the vapor and others, such as Fe, fractionate into the liquid. According to fluid inclusion analyses, such preferential fractionation between coexisting dense vapor and hypersaline liquid is significant. However, very few experiments designed to investigate this phenomenon have been undertaken for conditions approximating those of ore-forming systems, and consequently the controls of such partitioning are still poorly understood. Nonetheless, it is clear from thermodynamic theory and demonstrated by experimental partitioning studies that selective element fractionation vanishes as pressure-temperature conditions approach the critical point of the system (i.e., where the properties of liquid and vapor approach each other, as is common in boiling subsea-floor systems).

It follows from these basic conclusions that vapor transport and selective ore-metal enrichment are geologically most important in those regions of pressure-temperature-composition space where two hydrothermal fluids with strongly contrasting properties coexist at elevated pressure. Such conditions prevail in hot and saline magmatic-hydrothermal systems at depths of 1 to 5 km. Based on thermochemical considerations and geologic observations of specific porphyry-style and epithermal ore deposits, we conclude that vapor of highly variable density (typically 0.05–0.5 g/cm³) plays a central role

in the transport and local enrichment of the ore metals as well as sulfur.

The formation of porphyry Cu-Au and epithermal Au-Ag deposits can be envisaged as a continuous process driven by the cooling of a large hydrous magma chamber. A single-phase vapor of low density and very low salinity is released from the shallowest part of an intrusion and may immediately condense a small proportion of brine or precipitate solid halite. On ascent, the fumarolic vapor expands and cools, producing advanced argillic alteration and residual quartz, and locally also Hg, Sn, or Au-Ag mineralization. As the magma cools and a solid carapace develops beneath a few kilometers of overburden, fluids of higher density and salinity exsolve from the underlying magma. This favors metal hydration and complexation in a vapor that condenses a small proportion of brine during ascent and cooling. If the fracture permeability of the overlying rocks permits further expansion of the resulting vapor, copper and gold will be deposited together in a porphyry-type ore deposit, because the solubility of the metals decreases rapidly with decreasing vapor density. High-grade epithermal gold deposits are most efficiently formed by low-salinity aqueous liquids derived by contractive cooling of dense metal-enriched magmatic vapor. Ideal physical and chemical conditions are met where magmatic vapor first loses some Fe-enriched brine and then contracts to a gold- and sulfur-rich liquid of low to intermediate salinity by cooling at elevated pressure above the critical curve of the fluid system. This is most likely to occur during late stages in the cooling of a magmatic-hydrothermal system, when brine-vapor separation takes place at a depth of several kilometers above an even deeper magmatic fluid source. In partly eroded systems, such a fluid evolution is represented by slightly earlier potassic alteration and porphyry-style mineralization, cut by quartz-sericite-pyrite veins acting as fluid channelways for low-salinity fluids en route to overlying epithermal ore deposits.

Testing the geologic processes discussed in this paper will require much more experimentation to determine the speciation of metals in the vapor phase and their partitioning between liquid and vapor, as well as new measurements of the P-V-T properties of appropriate fluid systems. In conjunction with continued field-based studies of mineral paragenesis and microanalysis of fluid inclusions sampled in paragenetic context, such experimental data will permit the numerical modeling of two-phase fluid flow and fluid-rock reaction required to understand the dynamic processes of intrusion-related ore formation. It is our hope that these process models will eventually lead to new exploration tools with which to better predict the location and composition of economic orebodies within large magmatic-hydrothermal systems.

Acknowledgments

Many of the ideas and much of the information presented in this paper come from members of our research groups at McGill University and ETH Zürich. We would particularly like to acknowledge the contributions of A. Migdisov, T. Driesner, M. Landtwing, S. Archibald, T. Pettke, K. Rempel, W. Halter, K. Kouzmanov, and O. Nadeau from these groups. We thank J. Hanley, V. Lüders, and G. Pokrovski for discussion and access to data prior to publication. The manuscript has benefited from thoughtful reviews by H. Barnes,

J. Hedenquist, R. Henley, S. Kesler, J. Mavrogenes, H. Shinohara, and J. Webster. Financial support was provided by Natural Sciences and Engineering Research Council (NSERC) discovery and collaborative research grants to AEW-J and funding by the Swiss National Science Foundation to CAH.

September 6, November 11, 2005

REFERENCES

- Abraham M.H., and Matteoli E., 1983, Calculation of the thermodynamics of solvation of gaseous univalent ion in water from 273 to 573 K: *Journal of the Chemical Society Faraday Transactions*, v. 179, p. 2781–2800.
- Alderton, D.H.M., and Fallick, A.E., 2000, The nature and genesis of gold-silver-tellurium mineralization in the Metaliferi Mountains of western Romania: *ECONOMIC GEOLOGY*, v. 95, p. 495–515.
- Archibald, S.M., Migdisov A.A., and Williams-Jones A.E., 2001, The stability of Au-chloride complexes in water vapor at elevated temperatures and pressures: *Geochimica et Cosmochimica Acta*, v. 65, p. 4413–4423.
- 2002, An experimental study of the stability of copper chloride complexes in water vapor at elevated temperatures and pressures: *Geochimica et Cosmochimica Acta*, v. 66, p. 1611–1619.
- Armellini, F.J., and Tester, J.W., 1993, Solubility of sodium chloride and sulfate in sub- and supercritical water vapor from 450–550°C and 100–250 bars: *Fluid Phase Equilibria*, v. 84, p. 123–142.
- Arribas, A.J., 1995, Characteristics of high-sulfidation epithermal deposits, and their relation to magmatic fluid: *Mineralogical Association of Canada Short Course Series*, v. 23, p. 419–454.
- Arribas A., Cunningham, C.G., Rytuba, J.J., Rye, R.O., Kelly, W.C., Podwysoki, M.H., McKee, E.H., and Tosdal, R.M., 1995, Geology, geochronology, fluid inclusions, and isotope geochemistry of the Rodalquilar gold alunite deposit, Spain: *ECONOMIC GEOLOGY*, v. 90, p. 795–822.
- Audétat, A., and Pettke, T., 2003, The magmatic-hydrothermal evolution of two barren granites: A melt and fluid inclusion study of the Rito del Medio and Canada Pinabete plutons in northern New Mexico (USA): *Geochimica et Cosmochimica Acta*, v. 67, p. 97–121.
- Audétat, A., Günther, D., and Heinrich, C.A., 1998, Formation of a magmatic-hydrothermal ore deposit: Insights with LA-ICP-MS analysis of fluid inclusions: *Science*, v. 279, p. 2091–2094.
- 2000, Causes for large-scale metal zonation around mineralized plutons: Fluid inclusion LA-ICP-MS evidence from the Mole Granite, Australia: *ECONOMIC GEOLOGY*, v. 95, p. 1563–1581.
- Baker, T., Van Achtenberg, E., Ryan, C.G., and Lang, J.R., 2004, Composition and evolution of ore fluids in a magmatic-hydrothermal skarn deposit: *Geology*, v. 32, p. 117–120.
- Barnes, H.L., and Seward, T.M., 1997, Geothermal systems and mercury deposits in Barnes, H.L. ed., *Geochemistry of hydrothermal ore deposits*, 3rd ed.: New York, John Wiley and Sons, p. 699–736.
- Barrett, T.J., and Anderson, G.M., 1987, The solubility of sphalerite in 1–5 m NaCl solutions to 300°C: *Geochimica et Cosmochimica Acta*, v. 52, p. 813–820.
- Benning, L.G., and Seward, T.M., 1996, Hydrosulphide complexing of Au(I) in hydrothermal solutions from 150 to 400°C and 500 to 1500 bars: *Geochimica et Cosmochimica Acta*, v. 60, p. 1849–1971.
- Berger, B.R., and Henley, R.W., 1989, Advances in the understanding of epithermal gold-silver deposits, with special reference to the western United States: *ECONOMIC GEOLOGY MONOGRAPH* 6, p. 405–423.
- Bernard, A., 1985, Les mécanismes de condensation des gaz volcaniques—chimie minéralogique et équilibre des phases condensées majeures et mineures: Unpublished Ph.D. thesis, Belgium, University of Brussels, 195 p.
- Bernard, A., Symonds, R.B., and Rose, W.L., 1990, Volatile transport and deposition of Mo, W and Re in high temperature magmatic fluids: *Applied Geochemistry*, v. 5, p. 317–326.
- Bischoff, J.L., 1991, Densities of liquids and vapors in boiling sodium chloride-water solutions: A PVTX summary from 300° to 500 °C: *American Journal of Science*, v. 291, p. 309–338.
- Bischoff, J.L., Rosenbaum, R.J., and Pitzer, K.S., 1986, The system NaCl-H₂O: Relations of vapor-liquid near the critical temperature of water and of vapor-liquid-halite from 300 to 500°C: *Geochimica et Cosmochimica Acta*, v. 50, p. 1437–1444.
- Bodnar, R.J., 1995, Fluid-inclusion evidence for a magmatic source for metals in porphyry copper deposits: *Mineralogical Association of Canada Short Course Series*, v. 23, p. 139–152.
- Bodnar, R.J., Burnham, C.W., and Sterner, S.M., 1985, Synthetic fluid inclusions in natural quartz. III. Determination of phase equilibrium properties in the system H₂O-NaCl to 1000°C and 1500 bars: *Geochimica et Cosmochimica Acta*, v. 49, p. 1861–1873.
- Brimhall, G.H., and Ghiorso, M.S., 1983, Origin and ore-forming consequences of the advanced argillic alteration process in hypogene environments by magmatic gas contamination of meteoric fluids: *ECONOMIC GEOLOGY*, v. 78, p. 73–90.
- Browne, P.R.L., Roedder, E., and Wodzicki, A., 1974, Comparison of past and present geothermal waters, from a study of fluid inclusions, Broadlands field, New Zealand: *EOS*, v. 55, p. 456.
- Burnham, C.W., 1979, Magmas and hydrothermal fluids, in Barnes, H.L., ed., *Geochemistry of hydrothermal ore deposits*, 2nd ed.: New York, Wiley and Sons, p. 71–136.
- Candela, P.A., 1989a, Magmatic ore-forming fluids: Thermodynamic and mass transfer calculations of metal concentrations: *Reviews in Economic Geology*, v. 4, p. 203–221.
- 1989b, Felsic magmas, volatiles, and metallogenesis: *Reviews in Economic Geology*, v. 4, p. 223–233.
- Candela, P.A., and Holland, H.D., 1986, A mass-transfer model for copper and molybdenum in magmatic hydrothermal systems—the origin of porphyry-type ore deposits: *ECONOMIC GEOLOGY*, v. 81, p. 1–19.
- Candela, P.A., and Piccoli, P.M., 1995, Model ore-metal partitioning from melts into vapor and vapor/brine mixtures: *Mineralogical Association of Canada Short Course Series*, v. 23, p. 101–127.
- Cathelineau, M., Marignac, C., Boiron, M.C., Gianelli, and G. Puxeddu, M., 1994, Evidence for Li-rich brines and early magmatic fluid-rock interaction in the Larderello geothermal system: *Geochimica et Cosmochimica Acta*, v. 58, p. 1083–1099.
- Chaplygin, I., Safanov, Y., Mozgova, N., and Yudovskaya, M., 2005, New type of rare metal mineralization: Deposition of metals in high temperature vapor system of Kudryav volcano, Iturup Island, Kuriles, Russia [abs]: *Geochimica et Cosmochimica Acta*, v. 69, p. A734.
- Chouinard, A., Williams-Jones, A.E., Leonardson, R.W., Hodgson, C.J., Silva P., Téllez C. Vega, J., and Rojas, F., 2005a, Geology and genesis of the multistage high-sulfidation epithermal Pascua Au-Ag-Cu deposit, Chile and Argentina: *ECONOMIC GEOLOGY*, v. 100, p. 463–490.
- Chouinard, A., Paquette, J.P., and Williams-Jones, A.E., 2005b, Crystallographic controls on trace element incorporation in auriferous pyrite from the epithermal high-sulfidation Pascua deposit, Chile-Argentina: *Canadian Mineralogist*, v. 43, p. 951–963.
- Cline, J.S., 1995, Genesis of porphyry copper deposits: The behaviour of water, chloride and copper in crystallizing melts: *Arizona Geological Society Digest*, v. 20, p. 69–82.
- Cline, J.S., and Bodnar, R.J., 1991, Can economic porphyry copper mineralization be generated by a typical calc-alkaline melt?: *Journal of Geophysical Research*, v. 96, p. 8113–8126.
- Damman, A.H., Kars, S.M., Touret, J.L.R., Rieffe, E.C., Kramer, J., Vis, R.D., and Pintea, I., 1996, PIXE and SEM analyses of fluid inclusions in quartz crystals from the K-alteration zone of the Rosia Poieni porphyry-Cu deposit, Apuseni mountains, Rumania: *European Journal of Mineralogy*, v. 8, p. 1081–1096.
- Davey, H.A., and van Moort, J.C. 1987, Current mercury deposition at Ngava Springs, New Zealand: *Applied Geochemistry*, v. 1, p. 75–93.
- Delmelle, P., and Bernard, A., 1994, Geochemistry, mineralogy, and chemical modeling of the acid crater lake of Kawah Ijen volcano, Indonesia: *Geochimica et Cosmochimica Acta*, v. 58, p. 2445–2460.
- Driesner, T., and Heinrich, C. A., 2006, The system NaCl-H₂O. I. Correlation formulae for phase relations in temperature-pressure-composition space from 0 to 1000°C, 0 to 50000 bar, and 0 to 1 X_{NaCl}: *Geochimica et Cosmochimica Acta*, in press.
- Drummond, S.E., and Ohmoto, H., 1985, Chemical evolution and mineral deposition in boiling hydrothermal systems: *ECONOMIC GEOLOGY*, v. 80, p. 126–147.
- Duffield, W.A., Reed, B.L., and Richter, D.H., 1990, Origin of rhyolite-hosted tin mineralization: Evidence from the Taylor Creek rhyolite, New Mexico: *ECONOMIC GEOLOGY*, v. 85, p. 392–398.
- Eastoe, C.J., 1978, Fluid inclusion study of the Panguna porphyry copper deposit, Bougainville, Papua-New-Guinea: *ECONOMIC GEOLOGY*, v. 73, p. 721–748.
- 1982, Physics and chemistry of the hydrothermal system at the Panguna porphyry copper deposit, Bougainville, Papua New Guinea: *ECONOMIC GEOLOGY*, v. 77, p. 127–153.

- Ellis, J.A., 1979, Explored geothermal systems, in Barnes, H.L., ed., *Geochemistry of hydrothermal ore deposits*, 2nd ed.: New York, Wiley and Sons, p. 632–683.
- Etminan, H., 1977, Le porphyre cuprifère de Sar Cheshmeh (Iran); rôle des phases fluides dans les mécanismes d'altération et de minéralisation: Unpublished Ph.D. thesis, France, Mémoire Science, Terre Université Nancy, v. 34, 249 p.
- Fournier, R.O., 1999, Hydrothermal processes related to movement of fluid from plastic into brittle rock in the magmatic-epithermal environment: *ECONOMIC GEOLOGY*, v. 94, p. 1193–1211.
- Galobrades, J.F., Van Hare, D.R., and Rogers, L.B., 1981, Solubility of sodium chloride in dry steam: *Journal of Chemical Engineering Data*, v. 26, p. 363–366.
- Gammons, C.H., and Williams-Jones, A.E., 1995, Solubility of Au-Ag alloy + AgCl in HCl/NaCl solutions at 300°C: New data on the stability of Au(I) chloride complexes: *Geochimica et Cosmochimica Acta*, v. 59, p. 3453–3468.
- 1997, Chemical mobility of gold in the porphyry-epithermal environment: *ECONOMIC GEOLOGY*, v. 92, p. 45–59.
- Gemmell, J.B., 1987, Geochemistry of metallic trace elements in fumarole condensates from Nicaraguan and Costa Rican volcanoes: *Journal of Volcanological and Geothermal Research*, v. 33, p. 161–181.
- Giggenbach, W.F., 1992, Magma degassing and mineral deposition in hydrothermal systems along convergent plate boundaries: *ECONOMIC GEOLOGY*, v. 87, p. 1927–1944.
- Giggenbach, W.F., and Matsuo S., 1991, Evaluation of results from the second and third IAVCEI field workshops on volcanic gases, Mt. Usu, Japan, and White Island, New Zealand: *Applied Geochemistry*, v. 7, p. 125–141.
- Gustafson, L.B., and Hunt, J.P., 1975, Porphyry copper-deposit at El-Salvador, Chile: *ECONOMIC GEOLOGY*, v. 70, p. 857–912.
- Halter, W.E., Heinrich, C.A., and Pettke, T., 2005, Magma evolution and the formation of porphyry Cu-Au ore fluids: Evidence from silicate and sulphide melt inclusions: *Mineralium Deposita*, v. 39, p. 845–863.
- Hanley, J., Mungall, J., Pettke, T., Spooner, E.T.C., and Bray, C.J., 2005, Ore metal redistribution by hydrocarbon—brine and hydrocarbon—halide melt phases, North Range footwall of the Sudbury Igneous Complex, Ontario, Canada: *Mineralium Deposita*, v. 40, p. 237–256.
- Hedenquist, J.W., Simmons, S.F., Giggenbach, W.F., and Eldridge, C.S., 1993, White-Island, New-Zealand, volcanic-hydrothermal system represents the geochemical environment of high-sulfidation Cu and Au ore deposition: *Geology*, v. 21, p. 731–734.
- Hedenquist, J.W., Aoki, M., and Shinohara, H., 1994, Flux of volatiles and ore-forming metals from the magmatic-hydrothermal system of Satsuma Iwojima volcano: *Geology*, v. 22, p. 585–588.
- Hedenquist, J.W., Arribas, A., and Reynolds, T.J., 1998, Evolution of an intrusion-centered hydrothermal system: Far Southeast-Lepanto porphyry and epithermal Cu-Au deposits, Philippines: *ECONOMIC GEOLOGY*, v. 93, p. 373–404.
- Heinrich, C.A., 2005, The physical and chemical evolution of low- to medium-salinity magmatic fluids at the porphyry to epithermal transition: A thermodynamic study: *Mineralium Deposita*, v. 39, p. 864–889.
- Heinrich, C.A., Ryan, C.G., Mernagh, T.P., and Eadington, P.J., 1992, Segregation of ore metals between magmatic brine and vapor—a fluid inclusion study using PIXE microanalysis: *ECONOMIC GEOLOGY*, v. 87, p. 1566–1583.
- Heinrich, C.A., Günther, D., Audétat, A., Ulrich, T., and Frischknecht, R., 1999, Metal fractionation between magmatic brine and vapor, determined by microanalysis of fluid inclusions: *Geology*, v. 27, p. 755–758.
- Heinrich, C., Driesner, T., Stefánsson, A., and Seward, T.M., 2004, Magmatic vapor contraction and the transport of gold from porphyry to epithermal ore deposits: *Geology*, v. 39, p. 761–764.
- Henley, R.W., and Ellis, J.W., 1983, Geothermal systems ancient and modern; a geochemical review: *Earth Science Reviews*, v. 19, p. 1–50.
- Henley, R.W., and McNabb, A., 1978, Magmatic vapor plumes and ground-water interaction in porphyry copper emplacement: *ECONOMIC GEOLOGY*, v. 73, p. 1–20.
- Hildenbrand, D.L., and Lau, K.H., 1996, Thermochemistry of gaseous AgCl, Ag₃Cl₃, and CuCl: *High Temperature and Material Sciences*, v. 35, p. 11–20.
- Kavaleris, I., 1994, High Au, Ag, Mo, Pb, V, and W content of fumarole deposits at Merapi volcano, central Java, Indonesia: *Journal of Geochemical Exploration*, v. 50, p. 479–491.
- Kehayov, R., Bogdanov, K., Fanger, L., von Quadt, A., Pettke, T., and Heinrich, C.A., 2003, The fluid chemical evolution of the Elatiste porphyry Cu-Au-PGE deposit, Bulgaria, in Eliopoulos, D.G., ed., *Mineral exploration and sustainable development*: Rotterdam, Millpress, p. 1173–1176.
- Kelley, D.S., Robinson, P.T., and Malpas, J.G., 1992, Processes of brine generation and circulation in the oceanic crust—fluid inclusion evidence from the Troodos Ophiolite, Cyprus: *Journal of Geophysical Research-Solid Earth*, v. 97, p. 9307–9322.
- Kevan, L., Hase, H., and Kawabata, K., 1977, Silver atom solvation and desolvation in ice matrices: Electron spin resonance studies of radiation-produced silver atoms formed at 4 K: *Journal of Chemical Physics*, v. 66, p. 3834–3835.
- Korzinsky, M.A., Takchenko, S.I., Shmulovich, K.I., Taran, Y.A., and Steinberg, G.S., 1994, Discovery of a pure rhenium mineral at Kudriavitsky volcano: *Nature*, v. 369, p. 51–52.
- Kostova, B., Pettke, T., Driesner, T., Petrov, P., and Heinrich, C.A., 2004, LA ICP-MS study of fluid inclusions in quartz from the Yuzhna Petrovitsa deposit, Madan ore field, Bulgaria: *Schweizerische Mineralogische und Petrographische Mitteilungen*, v. 84, p. 25–36.
- Krabbes, G., and Oppermann, H., 1977, Die Thermodynamik der Verdampfung der Kuper(I)-Halogenide: *Zeitschrift für anorganische und allgemeine Chemie*, v. 435, p. 33–44.
- Krauskopf, K.B., 1957, The heavy metal content of magmatic vapor at 600°C: *ECONOMIC GEOLOGY*, v. 52, p. 786–807.
- 1964, The possible role of volatile metal compounds in ore genesis: *ECONOMIC GEOLOGY*, v. 59, p. 22–45.
- Landis, G.P., and Rye, R.O., 2005, Characterization of gas chemistry and noble-gas isotope ratios of inclusion fluids in magmatic-hydrothermal and magmatic-steam alunite: *Chemical Geology*, v. 215, p. 155–184.
- Landtwin, M.R., Heinrich, C.A., Pettke, T., Halter, W.E., Redmond, P.B., Einaudi, M.T., and Kunze, K., 2005, Copper deposition during quartz dissolution by cooling magmatic-hydrothermal fluids: The Bingham porphyry: *Earth and Planetary Science Letters*, v. 235, p. 229–243.
- Le Guern, F., 1988, Ecoulements gazeux réactifs à hautes températures, mesures et modélisation: Unpublished Ph.D. thesis, University of Paris, 314 p.
- Le Guern, F., and Bernard, A., 1982, A new method for sampling and analyzing sublimates: Application to Merapi volcano, Java: *Journal of Volcanological and Geothermal Research*, v. 12, p. 133–146.
- Lowenstern, J.B., 1995, Applications of silicate melt inclusions to the study of magmatic volatiles: *Mineralogical Association of Canada Short Course Volume 23*, p. 71–99.
- 1994, Dissolved volatile concentrations in an ore-forming magma: *Geology*, v. 22, p. 893–896.
- Lowenstern, J.B., Mahood, G.A., Rivers, M.L., and Sutton, S.R., 1991, Evidence for extreme partitioning of copper into a magmatic vapor-phase: *Science*, v. 252, p. 1405–1409.
- Lüders, V., Rickers, K., Banks, D.A., and Meston, L., 2005, Fluid inclusion evidence for extreme element partitioning during subcritical phase separation: Abstracts of the 15th Annual Goldschmidt Conference, *Geochimica et Cosmochimica Acta*, v. 69, p. A734.
- Martinez, J.M., Pappalardo, R.R., and Marcos, E.S., 1997, Study of the Ag^I hydration by means of a semicontinuum quantum-chemical solvation model: *Journal of Physical Chemistry A*, v. 101, p. 4444–4448.
- Martynova, O.I., 1964, Some problems of the solubility of involatile inorganic compounds in water vapor at high temperatures and pressures: *Russian Journal of Physics and Chemistry*, v. 38, p. 587–592.
- Mavrogenes, J.A., Berry, A.J., Newville, M., and Sutton, S.R., 2002, Copper speciation in vapor-phase fluid inclusions from the Mole Granite, Australia: *American Mineralogist*, v. 87, p. 1360–1364.
- Menyailov, I.A., and Nikitina, L.P., 1980, Chemistry and metal contents of magmatic gases: The new Tolbachik volcanoes gas (Kamchatka): *Bulletin of Volcanology*, v. 43, p. 197–207.
- Migdisov, A.A., and Williams-Jones, A.E., 2005, An experimental study of cassiterite solubility in HCl-bearing water vapor at temperatures up to 350°C. Implications for tin ore-formation: *Chemical Geology*, v. 217, p. 29–40.
- Migdisov, A.A., Williams-Jones, A.E., and Suleimenov, O.M., 1999, The solubility of chlorargyrite (AgCl) in water vapor at elevated temperatures and pressures: *Geochimica et Cosmochimica Acta*, v. 63, p. 3817–3827.
- Millner, T., and Neugebauer, J., 1949, Volatility of the oxides of tungsten and molybdenum in the presence of water vapour: *Nature*, v. 163, p. 601–602.
- Möller, P., Dulski, P., and Morteau, G., 2003, Partitioning of rare earth elements, yttrium, and some major elements among source rocks, liquid and vapor of Larderello-Travale geothermal field, Tuscany (Central Italy): *Geochimica et Cosmochimica Acta*, v. 67, p. 171–183.
- Muntean, J.L., and Einaudi, M.T., 2000, Porphyry gold deposits of the Refugio district, Maricunga belt, northern Chile: *ECONOMIC GEOLOGY*, v. 95, p. 1445–1472.
- 2001, Porphyry-epithermal transition: Maricunga belt, northern Chile: *ECONOMIC GEOLOGY*, v. 96, p. 743–772.

- Muramatsu, Y., and Komatsu, R. 1999, Microthermometric evidence for the formation of Ca-rich hypersaline brine and CO₂-rich fluid in the Mori geothermal reservoir, Japan: *Resource Geology*, v. 49, p. 27–37.
- Naboko, S.I., 1964, Contemporary volcanoes and gas hydrothermal activity: *Geologiya SSSR*, v. 31, p. 323–387.
- Nagaseki, H., and Hayashi K., 2004, Vapor-liquid partitioning experiment of ore metals in boiling hydrothermal solutions using synthetic fluid inclusions [abs]: Society of Resource Geology Annual Meeting, Tokyo, June, 2004, Abstracts, p. 17 (in Japanese).
- Palenik, C.S., Utsunomiya, S., Reich, M., Kesler, S.E., Wang, L., and Ewing, R.C., 2004, Invisible gold revealed: Direct imaging of gold nanoparticles in a Carlin-type deposit: *American Mineralogist*, v. 89, p. 1359–1366.
- Palinkas, L., Strmic, S., Spangenberg, S., Prochaska, W., and Herlec, U., 2004, Ore-forming fluids in the Grüber orebody, Idrija mercury deposit, Slovenia: *Schweizerische Mineralogische und Petrographische Mitteilungen*, v. 84, p. 173–188.
- Palmer, D.A., Fernández-Prini, R.J., and Harvey, A.H., 2004a, Aqueous systems at elevated temperatures and pressures: New York, Elsevier Academic Press, p. 409–439.
- Palmer, D.A., Simonson, J.M., and Hensen, J.P., 2004b, Partitioning of electrolytes to steam and their solubilities in steam, in Palmer, D.A., Fernández-Prini, R.J. and Harvey, A.H., eds, *Aqueous systems at elevated temperatures and pressures*: New York, Elsevier Academic Press, p. 409–439.
- Pankratz, L.B., 1982, Thermodynamic properties of elements and oxides: U.S. Department of the Interior, Bureau of Mines, 509 p.
- 1984, Thermodynamic properties of halides: U.S. Department of the Interior, Bureau of Mines, 826 p.
- Peabody, C.E., and Einaudi, M.T., 1992, Origin of petroleum and mercury in the Culver-Baer cinnabar deposit, Mayacmas district, California: *ECONOMIC GEOLOGY*, v. 87, p. 1078–1103.
- Peterson, D.E., 1973, Sublimation thermodynamics and kinetics of cuprous-chloride. Pt. I: Vacuum balance-torsion experiments. Part II: Mass-spectrometer experiments: Unpublished Ph.D. dissertation, Lawrence, University of Kansas, 484 p.
- Pitzer, K.S., and Palaban, R.T., 1986, Thermodynamics of NaCl in steam: *Geochimica et Cosmochimica Acta*, v. 50, p. 1445–1454.
- Pokrovski, G., 2004, Vapor-liquid partitioning of metals at hydrothermal conditions [abs]: *Geochimica et Cosmochimica Acta*, Special Supplement, Abstracts of the 13th Annual V.M. Goldschmidt Conference, v. 68, p. A294.
- Pokrovski, G., Roux, J., and Harrichoury, J.-C., 2005, Fluid density control on vapour-liquid partitioning of metals in hydrothermal systems: *Geology*, v. 33, p. 657–660.
- Quisefit, J.P., Toutain J.P., Bergametti G., Javoy M., Cheyet B., and Person A., 1989, Evolution versus cooling of gaseous volcanic emissions from Momotombo volcano, Nicaragua: Thermochemical model and observations: *Geochimica et Cosmochimica Acta*, v. 53, p. 2591–2608.
- Ransome, F.L., 1907, The association of alunite with gold in the Goldfield district, Nevada: *ECONOMIC GEOLOGY*, v. 2, p. 667–692.
- Raymond, J., Williams-Jones, A.E., and Clark, J.R., 2005, Mineralization associated with scale and altered rock and pipe fragments from the Berlin geothermal field, El Salvador: Implications for metal transport in natural systems: *Journal of Volcanology and Geothermal Research*, v. 145, p. 81–96.
- Redmond, P.B., Einaudi, M.T., Inan, E.E., Landtwing, M.R., and Heinrich, C.A., 2004, Copper deposition by fluid cooling in intrusion-centered systems: New insights from the Bingham porphyry ore deposit, Utah: *Geology*, v. 32, p. 217–220.
- Rempel, K.U., Migdisov, A.A., and Williams-Jones, A.E., 2005, The solubility and speciation of molybdenum in water vapour at elevated temperatures and pressures: Implications for ore genesis: *Geochimica et Cosmochimica Acta*, v. 70, p. 687–696.
- Roedder, E., 1971, Fluid inclusion studies on the porphyry-type ore deposits at Bingham, Utah, Butte, Montana, and Climax, Colorado: *ECONOMIC GEOLOGY*, v. 66, p. 98–118.
- 1984, Fluid inclusions: Reviews in Mineralogy, v. 12, 644 p.
- Rusk, B., Reed, M.H., Dilles, J.H., and Klemm, L., 2004, Compositions of magmatic-hydrothermal fluids determined by LA-ICPMS of fluid inclusions from the porphyry copper-molybdenum deposit at Butte, Montana: *Chemical Geology*, v. 210, p. 173–199.
- Rye, R.O., 1993, The evolution of magmatic fluids in the epithermal environment—the stable isotope perspective: *ECONOMIC GEOLOGY*, v. 88, p. 733–753.
- Rye, R.O., Betke, P.M., and Wasserman, M.D., 1992, The stable isotope geochemistry of acid-sulfate alteration: *ECONOMIC GEOLOGY*, v. 87, p. 225–262.
- Saupé, A.F., and Arnold, M., 1992, Sulphur isotope geochemistry of the ores and country rocks at the Almadén mercury deposit, Ciudad Real, Spain: *Geochimica et Cosmochimica Acta*, v. 56, p. 3765–3780.
- Sawkins, F.J., and Scherckenbach, D.A., 1981, High copper content of fluid inclusions in quartz from northern Sonora: Implications for ore genesis theory: *Geology*, v. 9, p. 37–40.
- Schatz, O.J., Dolejs, D., Stix, J., Williams-Jones, A.E., and Layne, G.D., 2004, Partitioning of boron among melt, brine and vapor in the system haplogranite-H₂O-NaCl at 800°C and 100 Mpa: *Chemical Geology*, v. 210, p. 135–147.
- Seward, T.M., and Barnes, H.L., 1997, Metal transport by hydrothermal ore, in Barnes, H.L., ed., *Geochemistry of hydrothermal ore deposits*, 3rd ed.: New York, Wiley and Sons, p. 435–486.
- Seward, T.M., Henderson, C.M.B., Charnock, J.M., and Dobson, B.R., 1996, An X-ray absorption (EXAFS) spectroscopic study of aquated Ag⁺ in hydrothermal solutions to 350°C: *Geochimica et Cosmochimica Acta*, v. 60, p. 2273–2282.
- Seyfried, W.E., Seewald, J.S., Berndt, M.E., Ding, K., and Foustoukos, D.I., 2003, Chemistry of hydrothermal vent fluids from the Main Endeavour field, northern Juan de Fuca Ridge: Geochemical controls in the aftermath of June 1999 seismic events: *Journal of Geophysical Research*, B, Solid Earth and Planets, v. 108, 23 p.
- Shevkunov, S.V., 1996, The numerical modeling of the Ag⁺ and I⁻ ion hydration in a wide temperature interval: *Russian Journal of Electrochemistry* (translation of *Elektrokimiya*), v. 32, p. 867–878.
- Shmulovich, K., Heinrich, W., Möller, P., and Dulski, P., 2002, Experimental determination of REE fractionation between liquid and vapour in the systems NaCl-H₂O and CaCl₂-H₂O up to 450 °C: *Contributions to Mineralogy and Petrology*, v. 144, p. 257–273.
- Signorelli, S., and Carroll, M.R., 2000, Solubility and fluid-melt partitioning of Cl in hydrous phonolitic melts: *Geochimica et Cosmochimica Acta*, v. 64, p. 2851–2862.
- Silberman, M.L., and O'Neil, J.R., 1974, Stable isotope relations in epithermal Au-Ag deposits: *ECONOMIC GEOLOGY*, v. 69, p. 902–909.
- Sillitoe, R.H., 1983, Enargite-bearing massive sulfide deposits high in porphyry copper systems: *ECONOMIC GEOLOGY*, v. 78, p. 348–352.
- Sillitoe, R.H., and Bonham, H.F., 1990, Sediment-hosted gold deposits—distal products of magmatic-hydrothermal systems: *Geology*, v. 18, p. 157–161.
- Simon, A.C., Frank, M.R., Pettke, T., Candela, P.A., Piccoli, P.M., and Heinrich, C.A., 2005a, Gold partitioning in melt-vapor-brine systems: *Geochimica et Cosmochimica Acta*, v. 69, p. 3321–3335.
- Simon, A.C., Pettke, T., Candela, P.A., Piccoli, P.M., and Heinrich, C.A., 2005b, Magnetite solubility and iron transport in magmatic-hydrothermal environments: *Geochimica et Cosmochimica Acta*, v. 68, p. 4905–4914.
- Simon, A.C., Candela, P.A., Pettke, T., Piccoli, P.M., and Heinrich, C.A., 2005c, The effect of sulfur on melt–volatile phase partitioning of copper [abs]: Geological Society of America Annual Meeting, Salt Lake City, Abstract 65–4 (CD).
- Sourirajan, S., and Kennedy G.C., 1962, The system H₂O-NaCl at elevated temperatures and pressures: *American Journal of Science*, v. 260, p. 115–141.
- Stefánsson, A., and Seward, T.M., 2004, Gold(I) complexing in aqueous sulphide solutions to 500°C at 500 bar: *Geochimica et Cosmochimica Acta*, v. 68, p. 4121–4143.
- Stoffregen, R., 1987, Genesis of acid-sulfate Alteration and Au-Cu-Ag mineralization at Summitville, Colorado: *ECONOMIC GEOLOGY*, v. 82, p. 1575–1591.
- Stoiber, R.E., and Rose, W.I., Jr., 1974, Fumarole incrustations at active Central American volcanoes: *Geochimica et Cosmochimica Acta*, v. 38, p. 495–510.
- Styrikovich, M.A., 1969, Steam solutions: *Vestnik Akademii Nauk SSSR*, v. 39, p. 70–77.
- Symonds, R.B., Rose, W.I., Reed, M.H., Lichte, F.E., and Finnegan, D.L., 1987, Volatilization, transport and sublimation of metallic and non-metallic elements in high temperature gases at Merapi volcano, Indonesia: *Geochimica et Cosmochimica Acta*, v. 51, p. 2083–2101.
- Symonds, R.B., Rose, W.I., Bluth, G.J., and Gerlach, T.M., 1994, Volcanic-gas studies: Methods, results, and applications: Reviews in Mineralogy, v. 30, p. 1–66.
- Tagirov, V.K., Makarov, V.A., and Brukvin, V.A., 1993, Vapor composition and pressure over chlorides of silver and gold: *Metalli*, v. 5, p. 67–71.
- Taran, Y.A., Hedenquist J.W., Korzhinsky, M.A., Tkachenko S.I., and Shmulovich K.I., 1995, Geochemistry of magmatic gases from Kudryavy volcano, Iturup, Kuril Islands: *Geochimica et Cosmochimica Acta*, v. 59, p. 1749–1761.

Appendix (Cont.)

	Th ² (°C)	NaCl (wt % equiv)	Li (ppm)	B (ppm)	Na (wt %)	K (wt %)	Mn (wt %)	Fe (wt %)	Cu (ppm)	Zn (ppm)	As (ppm)	Rb (ppm)	Sb (ppm)	Cs (ppm)	Au (ppm)	Tl (ppm)	Pb (ppm)	Bi (ppm)
Vapor BLA-I (1/97A.2a) ^{1,3}			50±40		1±0.1	0.4±0.2	0.10	0.3±0.1	510±200			37±1		4±2		2		0.1
Brine BLA-I (1/97A.2b) ^{1,3}	700	58	40±20	130±50	12.4±1	11.7±0.7	1.3±0.1	15.5±1.5	4800±3900	7400±800		690±80	10±14	49±4		52±6	3300±100	14±2.5
Vapor BLA-I (1/97A.2b) ^{1,3}			30±40		0.30	0.2±0.1	0.03	0.6±0.7	1100±1700	170±100		14±3	2±2	1		1	72±24	0.6±0.4
Brine BLA-A (1/97A.1.3) ^{1,3}	430	40.3			12.3±1.2	7±2.2	1.01±0.1	10.9±0.3	2200±1200	4600±1100		360±60		25±15		26±5	1600±300	18.2±2
Vapor BLA-A (1/97A.1.3) ^{1,3}					1.1±0.52	0.5±0.3	0.01	0.6±0.3	1200±400	440±180		27±11		2±1			140±80	
Brine BLA-H (49-52.21/3 A) ^{1,3}	700	52	60±60		11±1.2	8.1±0.9	1.9±0.1	9.2±1.7	2600±900	5400±700		490±40		42±2		12±3	1700±120	
Vapor BLA-H (49-52.21/3 A) ^{1,3}					0.3±0.2	0.7±0.5	0.01	0.10	260±220	75±7		13±8		0			26±11	
Brine BLA-J (1/97B.3 J) ^{1,3}	700	65.5			10±0.9	13±0.1	2.3±0.4	22.1±2.8	500±600	8900±800		550±50		45±5		36±8	2800±200	11.3±0.9
Vapor BLA-J (1/97B.3 J) ^{1,3}					0.7±0.1	0.8±0.1	0.10	1.4±0.7	900±400	660±230		31±9		3±1		4±2	210±50	1.5±0.6
Brine BLA-K (45-61.3, 13/2 K) ^{1,3}	400	43			8.5±3.5	9.5±3.5	2.3±0.8	12.6±5.3	7700±6200	7500±4200		500±90		40±12		25±16	2300±1200	122±11.9
Vapor BLA-K (45-61.3, 13/2 K) ^{1,3}					0.6±0.1	0.5±0.1	0.10	0.6±0.3	3000±2200	280±20		26±4		5±1			99±25	5.7±0.3
Grasberg (Irian Jaya) porphyry-Cu-Au deposit (Henrich et al., 1999; Ulrich et al., 1999)																		
Brine all assemblages ⁴	680	73			16.2±1	15.4±4.7	2.4±0.8	13.5±3.5	2900±1300	13000±4500	21±13	960±240		71±34	0.3±0.2	32±9	5100±2600	22±22
Vapor all assemblages ⁴		7			3±1	1.4±0.2	0.2±0.1	1±0.5	9900±9900	1400±700	190±220	80±30		4±1	11±11	4±1	360±140	6.1±1.6
Bingham, Utah (Henrich et al., 1999; Landthving et al., 2005)																		
Single-phase A57-5589.5 ⁵	375				1.6	0.40	0.05	0.42	3500	330	130	390			1.0		210	
Brine D211-19 ⁵	375	43			11.0	7.80	0.42	5.61	6050	3080	51	450		0	2.1 (1)		3190	
Vapor D211-19 ⁵					1.6	0.60	0.03	0.51	8100	300	83	90		0	2.2 (1)		880	
Brine D211-19 ^{1,3}	426	47			12.0	7.92	0.34	5.64	2.52	2900					0.6		2400	12
Vapor D211-19 ^{1,3}					1.6	0.44	0.02	0.72	0.53	350					6.0		210	3.4
Brine, BING-2A late Mo vein ^{1,3}	470	40	300	600±300	9.8±1.9	8.7±3.1	0.5±0.3	3.8±1.8	1700±700	2900±1200	40±1	600±300		47±23		21±5	2100±600	10±24
Vapor, BING-2A late Mo vein ^{1,3}			200	1200±700	2.5±0.3	1±0.6	0.1±0.1	0.8±0.4	3000±3000	1200±700	140±80	70±40	100±100	24±23			1000±800	44±64
Butte (Montana) porphyry-Cu-Mo deposit (Rusk et al., 2004; Table 2, averages of several assemblages)																		
Liquid 11172- 2756 r=0.65	~625	2.7			0.7±0.1	0.3±0.1	0.005	0.2±0.1	4300±3100	180±40		17±5		6±4			20±8	
Liquid 11172- 3186 r=0.65	~600	2.5			0.7±0.2	0.2±0.1	0.009	0.1±0.1	900±890	100±33		13±3		6±4			29±21	
Vapor 11552- 6673 r=0.40	~400	4.1			0.8±0.2	0.8±0.2	0.050	0.2±0.1	9800±5800	540±510		33±9		6±4			58±24	

Appendix (Cont.)

	Th ²	NaCl (wt % equiv)	Li	B	Na	K	Mn	Fe	Cu	Zn	As	Rb	Sb	Cs	Au	Tl	Pb	Bi
	(°C)		(ppm)	(ppm)	(wt %)	(wt %)	(wt %)	(wt %)	(ppm)	(ppm)	(ppm)	(ppm)	(ppm)	(ppm)	(ppm)	(ppm)	(ppm)	(ppm)
Elastite (Bulgaria) porphyry Cu-(Au) deposit (Kehayov et al., 2003)																		
Brine early qtz- mt-bn-cpy vein ³	550	51			13.2	8.6	1.45	7.3	6900	2700	330	580		58			1700	14
Vapor early qtz- mt-bn-cpy vein ³					1.02	3.8	0.05	0.88	28000	150		30		3	1.2		100	53
Brine cpy-py ore stage ³	450	47			10.2	6.1	0.66	7.4	1300	1500	250	550		52			1101	20
Vapor cpy-py ore stage ³					1.12				11000						0.26			
Rito del Medio (New Mexico) barren pluton (Audétat and Pettke, 2003)																		
Single-phase intermed																		
Rito 5-2/CZ	425	4.5	510		1.3±0.1	0.9±0.2	0.2±0.1	0.10	260±80					6±1			50±1	
Brine Rito 8-D					5.2±0.4	3.7±0.3	6.8±0.7	1.6±0.2	1600±270	16000±7000		1300±100	80	1300±30			2200	248
miarolitic cavity ^{1,3}																		
Vapor Rito 8-D		3.7	3100±1700		1.1±0.1	0.40	0.50		245	930±70		50±1	15	70±20			140±30	19±1
Brine Rito 5-B																		
miarolitic cavity ^{1,3}	450	29.5	1100	800	6.7±0.5	3.6±0.7	5.6±0.7	1.9±0.1	866±12	7900±752	80	590±140	35	850±200			1265±191	208±45
Vapor Rito 5-B																		
miarolitic cavity ^{1,3}	?	2.1			0.8±0.1	0.3±0.1	0.30	0.10	187±87	816±61	89	35±3		51±15			103±23	25.5±3
Canada Pinabete (New Mexico) barren pluton (Audétat and Pettke, 2003)																		
Single-phase inter-																		
mediate Cana 2 ^{1,3}	410	3.9			1.2±0.2	0.4±0.1	0.10	0.18	110±40	440±80							60±10	7±1
Brine Cana 2 ^{1,3}	500	40	1100		15.8±0.5	1±1	0.40	5.5±0.8	80±40	8000±1000			12	24±5			1200±100	22±8
Vapor Cana 2 ^{1,3}		4.5			1.3	0.40	0.26	0.21	2000	600			2.6±1	13			60	13
Bismarck Zn(-Pb-Cu-Ag) skarn, Mexico (Baker et al., 2004)																		
Brine average	~500	~ 47			Cl=29%	6.10	0.81	0.61	90	3100	440						3400	
Vapor average					Cl=1.6%	1.10	0.12	0.15	400	800	440						2500	
Single-phase near-																		
critical density	~400	~ 9.6			Cl=3.1%	1.10	0.03	0.06	190	450	80						730	
Madan (Bulgaria) Moglata Pb-Zn vein and manto deposit, quartz predating ore deposition (Heinrich et al., 1999)																		
Liquid MAD-7																		
isolated incls.	354	0.4	16	80	0.20	0.10	0.10	0.10								0.5±0.2	5±7	
Vapor MAD-7																		
isolated incls.	~350	0.4	120		0.2±0.1	0.10	0.10	0.10	110±120			6±3		3±3			90±110	

¹ Low-density vapor inclusions trapped together with coeval brine inclusions are listed on adjacent lines indicated by identical sample numbers² Temperature of homogenization to liquid phase corresponds closely to the entrapment temperature³ Fluid inclusions representing a single boiling trail trapped along a plane⁴ Fluid inclusions representing several boiling trails⁵ Average for all inclusions analyzed⁶ Averages for all coexisting brine and vapor inclusions in the sample; vapor inclusions have a density <0.2 g/cm³ and were observed to homogenize; single-phase fluid inclusions from Bingham, Rito del Medio, Canada Pinabete, and some from Butte homogenize mainly by the fading of the meniscus reflecting near-critical behavior; the homogenization temperature represents a minimum trapping temperature